LAPORAN AKHIR PROJEK PENYELIDIKAN
FRGS VOT: 78077

Algorithm of the Effect of g-Jitter on Free Convection Adjacent to a Stretching Sheet

Sharidan Shafie
Jabatan Matematik, Fakulti Sains,
Universiti Teknologi Malaysia

ACKNOWLEDGEMENT

First and foremost, my thanks go to Allah Almighty for graciously blessing me with the ability to undertake and finally complete this work. I would like to acknowledge Universiti Teknologi Malaysia for the financial support (FRGS) throughout the course of my research. My sincere thanks to all my colleagues, friends and students who kindly provided valuable and helpful comments in the preparation of this research.

ABSTRACT

g-Jitter characterizes a small fluctuating gravitational field brought about, among others, by crew movements and machine vibrations aboard spacecrafts or in other low-gravity environments such as the drop-tower and parabolic flights. Experimental studies have shown that in these low-gravity environments, g-jitter can induce appreciable convective flow that can be detrimental to certain experiments such as crystal growths and solidification processes.

In this research, mathematical models to study the effect of g-jitter on heat and mass transfer is developed. Specific problem considered revolve around the effect of g-jitter induced free convection, on the flow and heat transfer characteristics associated with a stretching vertical surface in a viscous and incompressible fluid. The velocity and temperature of the sheet are assumed to vary linearly with *x*, where *x* is the distance along the sheet. It is assumed that the gravity vector modulation is given by $g^*(t) = g_o\left[1+\varepsilon\cos(\pi\,\omega\,t)\right]k$, and the resulting non-similar boundary layer equations are solved numerically using an implicit finite-difference scheme. Results presented include fluid flow and heat transfer characteristics for various parametric physical conditions such as the amplitude of modulation, frequency of the single-harmonic component of oscillation, buoyancy force parameter and Prandtl number on the skin friction and Nusselt number. This theoretical investigation is useful in providing estimates of the tolerable effects of g-jitter which will help to ensure the design of successful experiments in low-gravity environments.

ABSTRAK

Ketar-g mencirikan suatu ayunan kecil medan raviti yang terhasil antaranya oleh gerakan angkasawan dan getaran mesin di dalam kapal angkasa atau di persekitaran graviti rendah yang lain misalnya di menara-jatuh dan penerbangan parabolik. Kajian secara eksperimen mendapati aliran olakan yang dijana oleh ketar-g di persekitaran graviti rendah, boleh mempengaruhi olakan yang boleh menjejaskan beberapa eksperimen seperti proses penghabluran dan proses pemejalan. Dalam kajian ini, model matematik dibina untuk mengkaji kesan ketar-g ke atas pemindahan haba dan jisim. Masalah yang dipertimbangkan merangkumi olakan bebas yang dijana oleh ketar-g terhadap pemindahan haba dan jisim ke atas permukaan regangan menegak dalam bendalir likat dan tidak mampat. Halaju dan suhu permukaan diandaikan berubah secara linear terhadap *x*, dengan *x* merupakan jarak disepanjang permukaan. Diandaikan juga perubahan vector gravity diberikan oleh $g^*(t) = g_o\left[1+\varepsilon\cos(\pi\,\omega\,t)\right]k$, dan persamaan terbitan separa tak linear diselesaikan secara analisis secara berangka dengan menggunakan skim beza terhingga tersirat. Penyelesaian diperolehi meliputi ciri-ciri aliran bendalir dan pemindahan haba dipaparkan secara grafik bagi perubahan amplitud, frekuensi bagi ayunan satu-harmonik, parameter daya apungan, nombor Prandtl untuk geseran kulit dan nombor Nusselt. Kajian teori ini penting untuk memberi anggaran tahap toleransi ketar-g yang boleh menjamin kejayaan eksperimen yang dijalankan di persekitaran graviti rendah.

TABLE OF CONTENTS

LIST OF TABLES

LIST OF FIGURES

LIST OF SYMBOLS

C	-	dimensional constant
d	-	dimensionless injection or suction parameter
f	-	dimensionless stream function
m	-	velocity exponent parameter
n	-	temperature exponent parameter
Nu	-	Nusselt number
Pr	-	Prandtl number
Re	-	Reynolds number
T	-	temperature
u	-	velocity component in x-direction
U_0	-	dimensional constant
v	-	velocity component in y-direction
x	-	coordinate in direction of surface motion
y	-	coordinate in direction normal to surface motion

Greek symbols

α	-	thermal diffusivity
η	-	dimensionless similarity variable
θ	-	dimensionless temperature
ν	-	kinematic viscosity
ψ	-	stream function

Subscripts

w	-	condition at the surface
∞	-	condition at ambient medium

Superscripts

‘	-	differentiation with respect to η

CHAPTER I

INTRODUCTION

1.1 Heat Transfer on Continuous Stretching Surface

Heat transfer is the energy interaction due to a temperature difference in a medium or between media. Heat is not a storable quantity and is defined as energy in transit due to a temperature difference. The applications of heat transfer are diverse, both in nature and in industry. Climatic changes, formation of rain and snow, heating and cooling of the earth surface, the origin of dew drops and fog, spreading of forest fires are some of the natural phenomena wherein heat transfer plays a dominant role. The importance of heat transfer in industry include heating and air conditioning of building, design of internal combustion engines, oil exploration, drying and processing of solid and liquid wastes.

It is no wonder J.B Joseph Fourier, the father of the theory of heat diffusion, made this remark in 1824: ‘Heat, like gravity, penetrates every substance of the universe; its rays occupy all parts of space. The theory of heat will hereafter forms one of the most important branches of general physics’, (Ghoshdastidar (2004)).

The problem of flow and heat transfer adjacent to a continuous stretching surface has attracted many researchers during the past few decades. This is because of its wide application in many manufacturing processes, such as continuous casting, glass fiber production, metal extrusion, hot rolling, manufacturing of plastic, paper production and wire drawing, (Chen (2000)). Both the kinematics of stretching and the heat transfer during such process have a decisive influence on the quality of the final product.

1.2 g-Jitter and Its Effects

Space experiments have revealed unknown or nonexistent effects on Earth which can be detrimental to certain experiments. For example, alloy solidification experiments conducted in space vehicles showed that the solute uniformity and defects formation in space grown crystals are strongly affected by free convection in the melt pool that arises as a result of the combined action of temperature and concentration gradients in the melt (Nelson (1991), Monti and Sovino (1998), Wilcox and Regel (2001)). These deleterious effects generally are considered to be a culprit for the quality of crystals grown in low-gravity environments (Alexander et. al. (1991), Kamotani et.al. (1995), Neumann (1990)). One of these effects is g-jitter or residual acceleration phenomena associated with the microgravity environment.

g-Jitter is defined as the inertia effects due to quasi-steady, oscillatory or transient accelerations arising from crew motions and machinery vibrations in parabolic aircrafts, space shuttles or other microgravity environments. Quasi-steady accelerations are accelerations which vary only little for periods longer than one minute, oscillatory accelerations are periodic with a characteristic frequency, while transient accelerations are non-periodic and typically have duration less than one second (Mell (2001)). g-Jitter characterizes a small fluctuating gravitational field, very irregular in amplitude, random in direction, and contains a broad spectrum of frequencies (Schneider and Straub (1989), Alexander et.al. (1991), Nelson (1991)). Its effects may be negligible in earthbound situations, but in a low-gravity environment, where heat and mass transfer in a fluid medium, in the absence of radiation, is expected to be affected only by pure diffusion, g-jitter can give rise to significant convective motions.

Studies on g-jitter effects indicate that convection in microgravity is related to the magnitude and frequency of g-jitter and to the alignment of the gravity field with respect to the growth direction or the direction of the temperature gradient (Pan et. al. (2002), Shu et. al (2001)). As an example, Ramos (2000) has shown that the thickness and axial velocity components, heat fluxes and interfacial temperature are

periodic functions of time whose amplitudes increase as the amplitude of the g-jitter increases, but decrease as the frequency of g-jitter increases. Results from Li (1996) show that the frequency and amplitude of the g-jitter all play an important role in determining the convective flow behaviour of the system. When the residual accelerations oscillate about the positive and negative of an axis, the orientation of this direction relative to the density gradient determines whether a mean flow is generated in the system.

g-Jitter has large effects on materials processing in space or in gravity-reduced environment. It can interact with the density gradients and result in both fluid flow and solute segregation. Wilcox and Regel (2001) has reviewed the microgravity effects on the material processing. They concluded that convection should result, that the amount of convection increases with increasing acceleration and decreasing frequency, and that it will significantly influence some materials processing operations. Alexander et al. (1991) found that the orientation of the residual gravity is a crucial factor in determining the suitability of the spacecraft environment as a means to suppress or eliminate unwanted effects caused by buoyant fluid motion in Bridgman's crystal growth experiment. These authors found that g-jitter affects the compositional uniformity of the growing crystal.

1.3 Significance of Research

The effect of g-jitter on experiments, compared to ideal zero gravity conditions, is largely unknown, especially in quantitative terms. It is therefore of great interest to quantitatively access acceptable acceleration levels for a given experiment such that the processes to be studied would not be appreciably distorted by the environment in which the experiments take place. Significant levels of g-jitter have been detected during space missions in which low-gravity experiments were being conducted. The problem has been approached from a numerical standpoint, one of the key results being that a relatively modest acceleration of $10^{-5}g_0$ (g_0 being the gravity on the surface or the Earth) can have a significant impact on solute

segregation (Pan et. al (2002)). This is true even though velocity magnitudes are several orders lower than under terrestrial conditions. Unfortunately, a complete experimental parametric study of this g-jitter problem is obviously impossible, so one has to rely on modelling to gain some insight into the question (Alexander et. al. (1991)).

Alexander (1997) has mentioned that theoretical models can be used effectively to predict the experiment sensitivity to g-jitter, provided the time-dependent nature of the g-jitter is properly characterized. His experimental work in the MEPHISTO (Material pour l'Etude des Phenomenes Interessant la Solidification sur Terre et n Orbite) furnace facility to observe the effect of g-jitter on segregation during directional solidification of tin-bismuth indicated that a "cause and effect" relationship between g-jitter and disturbances in the transport conditions can be clearly identified. These results are of significance for planning future low-gravity experiments, and analyzing the results of past experiments. Reliable prediction of g-jitter sensitivity based on models with proven experimental correlations can be used to optimize the limited time available for low-gravity experimentation, determine acceptable levels of g-jitter, and avoid unnecessary (expensive) design restrictions which might arise due to inaccurate predictions.

For materials science experiments conducted in low earth-orbit spacecraft, there are many open questions regarding experiment sensitivity to residual acceleration. Since sensitivity to g-jitter is an important consideration in the selection of optimal experiment operating conditions, it is imperative that these questions be answered so that the scientific return from such experiments is maximized. In order to obtain a more efficient engineering design in low-gravity conditions, more informations regarding the effect of g-jitter on fluid behaviour in low gravity environment is needed. The results of study should be helpful in understanding the g-jitter effects on fluid mechanics process in microgravity conditions and better engineering design could be made in the future.

1.4 Objectives and Scope of Research

The main objective of this project is to investigate theoretically the heat transfer coefficients on continuous stretching surface and the effect of g-jitter adjacent to a vertical stretching sheet. This involves the construction of suitable mathematical models by formulating the appropriate governing equations and choosing the right boundary conditions and then solving the resulting equations using both analytical and numerical means.

1.5 Report Outline

This report consists of six chapters including this introductory chapter, where we have presented the research background, objectives and significance of research. In Chapter 2, a literature review on the problems concerning the heat transfer on continuous stretching surface and the effect of g-jitter adjacent to a vertical stretching sheet presented and discussed. Chapter 3, concerned with numerical scheme used in this study, which is the Keller-box method. Keller and Cebeci (1972) reported that this method is very simple and accurate which is applicable to boundary layer flow problems. This method is chosen since it seem to be most flexible of the common methods, being easily adaptable to solving equation of any order (Cebeci and Bradshaw (1977)). One of the basic ideas of the Keller-box method is to write the governing equation in the form of a first order system.

In Chapter 4, we consider the problem of heat transfer coefficients on a continuous stretching surface. We will use the Keller-box method that has been described in Chapter 3 to solve this problem. Three cases of thermal boundary conditions, namely uniform surface temperature $(n = 0)$, variable surface temperature $(n \neq 0)$ and uniform heat flux $(n = (1-m)/2)$ are presented in the following three main section.

Chapter 5 is concerned with the effect of periodical gravity modulation, or g-jitter induced free convection, on the flow and heat transfer characteristics associated with a stretching vertical surface in a viscous and incompressible fluid. The velocity and temperature of the sheet are assumed to vary linearly with *x*, where *x* is the distance along the sheet. It is assumed that the gravity vector modulation is given by $g^*(t) = g_o\left[1+\varepsilon\cos(\pi\omega t)\right]k$, and the resulting non-similar boundary layer equations are solved numerically using an implicit finite-difference scheme. The effects of the amplitude of modulation, frequency of the single-harmonic component of oscillation, buoyancy force parameter and Prandtl number on the skin friction and Nusselt number are discussed in detail.

Finally the concluding chapter, Chapter 6, contains a summary of the main results of the report and several recommendations for future research.

CHAPTER II

LITERATURE REVIEW

2.1 Introduction

This chapter contains a literature review on two main topics to be investigated, namely in Section 2.2 studies concerning with continuous stretching surface is discussed and in Section 2.3 contains related research on the effect of g-jitter on vertical stretching sheet.

2.2 Continuous Stretching Surface

The flow and heat transfer stirred up by a continuous stretching surface entering the cooling viscous fluid is important in a practical engineering process. For example, materials which are manufactured by extrusion process and heat-treated substances proceeding between a feed roll and a wind-up roll can be classified as the continuous stretching surface. In order to get the top-grade property of the final product, the cooling procedure should be effectively controlled. There are three types of velocity and temperature distributions for problems involving continuous stretching surface namely self similar, power law and exponential form.

In the past few decades, the related investigation about stretching surface has never been interrupted. Sakiadis (1961) initiated the study of boundary layer flow over a continuous solid surface moving with constant speed. It was observed that the boundary layer growth is in the direction of motion of the continuous solid surface

and different from that of the Blasius flow past a flat plate. Crane (1970) gave similarity solution closed to an analytical form for steady 2D incompressible boundary layer flow caused by the stretching surface with linear velocity.

Banks (1983) discussed the flow field of stretching wall with a power law velocity variation for different values of velocity exponent. Grubka and Bobba (1985) studied the heat transfer characteristics of a continuous stretching surface with linear surface velocity and power law surface temperature for different value of Prandtl number and temperature exponent.

Ali (1994) who extended Bank's and Grubka work for continuous stretching surface problem. He investigates the heat transfer characteristics of a continuous stretching surface with power law velocity and temperature distribution. Three thermal boundary conditions of uniform surface temperature, variable surface temperature and uniform heat flux at the continuous stretching surface had been investigated.

Chen and Char (1988) has reported the heat transfer characteristics of a continuous stretching surface with power law surface temperature and power law surface heat flux variation with effect of suction or blowing. Ali (1995) has examined the effects of suction or injection for heat and flow in a quiescent fluid driven by a continuous stretched surface. He also used power law velocity and temperature variation with three thermal boundary condition for this problem. The thermal boundary condition that he used was the same with Ali (1994). It was shown that suction increased the heat transfer from surfaces whereas, injection cause a decrease in the heat transfer.

Rollins and Vajwavelu (1991) have investigated the heat transfer characteristics in a viscoelastic fluid over a continuous stretching surface with internal heat generation. Two cases were studied in this problem namely (i) the sheet with uniform surface temperature and (ii) the sheet with uniform wall heat flux. The solution and heat transfer characteristics were obtained in terms of Kummer's

Functions. They found for large values of Prandtl number a uniform approximation could be expressed in terms of parabolic cylinder functions in both cases.

Chen (1998) presented the numerical solutions of laminar mixed convection in boundary layers adjacent to vertical, continuously stretching sheets. The Keller-box method was used to solve this problem. The author studied the effect of thermal buoyancy on flow past a vertical, continuously stretching where the velocity and temperature variation was assumed power law form.

Magyari and Keller (1998) discussed heat and mass transfer in the boundary layer on an exponentially stretching continuous surface. They intended to complete the investigations by discussing a further type of similarity solution of the governing equations. Their solutions involve an exponential dependence of the similarity variable as well as the stretching velocity and the temperature distribution on the coordinate in the direction parallel to that of the stretching.

In 2001, Mohammadein and Rama studied the heat transfer characteristics of a laminar micropolar fluid boundary layer over a linearly stretching, continuous surface. They consider the effect of viscous dissipation and internal heat generation with self similar velocity and temperature variation.

Heat transfer characteristic of the separation boundary flow induced by a continuous stretching surface was reported by Magyari and Keller (1999). They discussed an exact-solvable case of separation flow characterized by an identically vanishing skin friction with power law velocity and temperature variation.

Tashtoush et al (2000) have examined the laminar boundary layer flow and heat transfer characteristics of a non-Newtonian fluid over a continuous stretching surface subject to power-law velocity and temperature distribution with suction or injection parameter. Their results was obtained numerically using fourth order Rungge-Kutta method to show suction and injection effect for uniform and cooled surface temperature.

Chen (2000) have investigated the flow and heat transfer characteristics associated with a heated, continuously stretching surface being cooled by a mixed convection flow. These problems also assume the velocity and temperature distribution is varying according to a power-law form subject to variable surface temperature and variable surface heat flux boundary condition. Their results show that the local Nusselt number is increased with increasing the velocity exponent for variable surface temperature case while the opposite trend is observed for the variable surface heat flux. The author also found that the local skin friction coefficient is increased for a decelerated stretching surface, while it decreased for an accelerated stretching surface.

Mechanical and thermal properties of the self similar boundary layer flow induced by continuous stretching surface with rapidly decreasing power law $(m < -1)$ and exponential velocity was studied by Maygari et al (2001).Ali (2004) who extend Magyari et al (2001) work for continuous stretching surface with different values of velocity exponent in the presence of the buoyancy force and the surface was moving vertically subject to power-law velocity.

Seddek and Salem (2005) examined the effect of thermal buoyancy on flow past a vertical continuous stretching surface with variable viscosity and variable thermal diffusivity. Their results showed that variable viscosity, variable thermal diffusivity, the velocity exponent parameter, the temperature had the significance influences on the velocity and temperature profiles, shear stress and Nusselt number in two cases air and water. The result was obtained numerically using the shooting method.

Partha et al (2005) presented a similarity solution for a mixed convection flow and heat transfer from an exponentially stretching surface subject to exponential velocity and temperature distribution. The influence of buoyancy along with viscous dissipation on the convective transport in the boundary layer region is analyzed.

Magyari and Keller (2006) studied the heat transfer characteristics of the laminar boundary layer flow induced by continuous stretching surface with prescribed skin friction subject to power law velocity and temperature variation.

Sanjayanand and Khan (2006) analyzed the effect of various physical parameters like viscoelastic parameter, Prandtl number, local Reynold number and Eckert number on various momentum, heat and mass transfer of boundary layer with second fluid characteristic over continuous stretching surface with exponential velocity and temperature distribution.

Recently Ishak et al (2007) studied the mixed convection on the stagnation point flow toward a vertical, continuously stretching sheet. They analyzed the effects of governing parameters on the flow and heat transfer characteristics for fixed value of Prandtl number. They found the dual solution exist in the neighborhood of the separation region.

Many authors have studied this problem. However they limited to some constraints on the surface velocity and temperature. Tsou et al (1967) have considered the continuous moving surface with constant velocity and temperature. Stretched surface with different velocity boundary condition and for various temperature boundaries at the surface was studied by Crane (1970), Grubka and Bobba (1985), Soundalgekar and Murty (1980) and Vleggar (1977).

Suction or injection of a stretched surface was introduced by Erickson et al (1966) and Fox et al (1968) for uniform surface velocity and temperature. Gupta and Gupta (1977) extended Erickson's work, in which the surface was moved with a linear speed for various values of parameters. Furthermore, linearly stretching surface subject to suction or injection was studied by Chen and Char (1998) for uniform wall temperature and heat flux.

In the classical convective heat transfer between solid wall and the fluid flow, usually the temperature or heat flux at the solid-fluid interface is prescribed over the entire interface. Physically, the condition of uniform surface temperature is achieved

by either violent mixing or a phase change, for example, boiling or condensation, on the other side of a thin wall that has a higher thermal conductivity. However, in certain engineering systems, the condition of constant surface temperature does not apply. For example, in the design of thermal insulation, material processing, and geothermal systems, it has been observed that natural convection can induce thermal stresses that lead to critical structural damage in the piping systems of nuclear reactors. But, an important practical and experimental circumstance in many forced, free and mixed convection flows is that generated adjacent to a surface dissipating heat uniformly.

The effect of uniform surface temperature and uniform heat flux gives much impact on heat transfer process. Thus, our first problem of this study is to investigate the heat transfer coefficients of a continuous stretching surface subjected to a uniform surface temperature, variable surface temperature and uniform heat flux, respectively.

2.3 The Effect of g-Jitter on Vertical Stretching Sheet

The production of sheeting material which includes both metal and polymer sheets arises in a number of industrial manufacturing processes. The fluid dynamics due to a stretching surface is important in many extrusion processes. Since the pioneering study by Crane (1970) who presented an exact analytical solution for the steady two-dimensional stretching of a surface in a quiescent fluid many authors have considered various aspects of this problem and obtained similarity solutions. Many researchers presented theoretical results on this problem. The papers by Magyari and Keller (1999, 2000), and Nazar et al. (2004) contain a good amount of references, but these studies pertain to forced convection flows only. On the other hand, problems involving the boundary layer flow due to a stretching surface in the vertical direction in a steady, viscous and incompressible fluid when the buoyancy forces are taken into account have been considered by Daskalakis (1993), Ali and Al-Yousef (1998), Chen (1998, 2000), Lin and Chen (1998) and Chamkha (1999).

However, only Kumari et al. (1996) have studied the unsteady free convection flow over a stretching vertical surface in an ambient fluid, where they considered both cases of constant surface temperature and constant heat flux.

It is known that in many situations the presence of a temperature gradient and a gravitational field can generate buoyancy convective flows. Recent technological implications have given rise to increased interest in oscillating natural and mixed convection driven by g-jitter forces associated with microgravity. In low-gravity or microgravity environments, it can be expected that the reduction or elimination of natural convection may enhance the properties and performance of materials such as crystals. However, aboard orbiting spacecrafts all objects experience low-amplitude perturbed accelerations, or g-jitter, caused by crew activities, orbiter manoeuvres, equipment vibrations, solar drag and other sources (Antar and Nuotio-Antar, (1993); Hirata et al. (2001)). There is a growing literature, which tries to characterize the g-jitter environment and the review articles by Alexander (1990) and Nelson (1991) give a good summary of earlier work on convective flows in viscous fluids. There have also been a number of studies which investigate the effect of g-jitter on flows involving viscous fluids and porous media, e.g. Amin (1988), Farooq and Homsy (1994), Li (1996), Pan and Li (1998), Rees and Pop (2000, 2001), and Chamkha (2003). However, to our best knowledge there has not been any study regarding g-jitter effects on stretching problems. Therefore, in this paper, we will study the behavior of g-jitter induced free convection of a viscous and incompressible fluid due to a surface, which is stretched in the vertical direction.

Following Rees and Pop (2000, 2001), we consider a simple model problem in which the gravitational field takes the form

$$g^*(t) = g_o\left[1+\varepsilon\cos(\pi\omega t)\right]k \tag{2.3.1}$$

where g_o is the time-averaged value of the gravitational acceleration $g^*(t)$ acting along the direction on the unit vector $\boldsymbol{k}$, ε is a scaling parameter, which gives the magnitude of the gravity modulation relative to g_o, t is the time and ω is the

frequency of oscillation of the *g*-jitter driven flow.

The effect of oscillating free convection is driven by g-jitter forces associated with a gravitational field given by equation (2.3.1) on the boundary layer flow over a vertical stretching surface. For many practical applications the stretching surfaces undergo cooling or heating that cause surface velocity and temperature variations. It is assumed here that the stretching velocity and the surface temperature vary linearly with the distance along the surface. In addition, it is assumed that the g-jitter field under consideration is spatially constant , otherwise varies harmonically with time. The governing partial differential equations are transformed into a non-dimensional form using similarity variables and then solved numerically using the Keller-box method which is an implicit finite-difference scheme.

Similarity solutions can be obtained for the special case when the amplitude of the modulation is zero and we have shown that solutions of these equations exist only for limited values of the negative buoyancy force parameter. Effects of the amplitude of modulation, frequency of the single-harmonic component of oscillation, buoyancy force parameter and Prandtl number on the skin friction and Nusselt number are discussed in detail.

CHAPTER III

THE KELLER-BOX METHOD

3.1 Introduction

This chapter discusses the details of the numerical scheme used in this study, which is the Keller-box method. Keller and Cebeci (1972) reported that this method is very simple and accurate which is applicable to boundary layer flow problems. This method is chosen since it seem to be most flexible of the common methods, being easily adaptable to solving equation of any order (Cebeci and Bradshaw (1977)). One of the basic ideas of the Keller-box method is to write the governing equation in the form of a first order system.

In Section 3.2 the discussion begins with the governing equations for the problem of the heat transfer characteristic of a continuous stretching surface. Then we discuss the finite difference method in Section 3.3. We shall use centered difference derivatives and average at the midpoints of net rectangle to get the finite difference equations. The finite difference equations are generally nonlinear algebraic equations. In this study, we linearize the resulting nonlinear algebraic equations using Newton's method. Full details of Newton's method will give in Section 3.4. In Section 3.5, we solve the linear system by the block-tridiagonal factorization method. This method is employed on the coefficient matrix of the finite difference equations. Finally, we discuss the choice of suitable starting conditions for the numerical computation in Section 3.6. This section include the determination of values y_∞, the selection of step size, as well as the assumptions of the initial velocity and temperature profiles.

3.2 Governing Equation

A steady two dimensional motion of incompressible viscous fluid due to a continuous stretching surface in a stationary fluid is governed by the continuity, momentum and energy equation under the boundary layer approximation are

Continuity equation,

$$\frac{\partial u}{\partial x}+\frac{\partial v}{\partial y}=0 \tag{3.2.1}$$

Momentum equation,

$$u\frac{\partial u}{\partial x}+v\frac{\partial u}{\partial y}=\nu\frac{\partial^2 u}{\partial y^2} \tag{3.2.2}$$

Energy equation,

$$u\frac{\partial T}{\partial x}+v\frac{\partial T}{\partial y}=\alpha\frac{\partial^2 T}{\partial y^2} \tag{3.2.3}$$

subject to boundary conditions

$$u=u_w(x),\ v=0 \text{ and } T=T_w(x) \quad \text{at } y=0, \tag{3.2.4a}$$

$$u=0 \quad \text{and } T=T_\infty \quad \text{at } y\to\infty \tag{3.2.4b}$$

The continuous stretching surface is assumed to have power-law velocity and temperature variations, that is $u_w(x)=U_0x^m$ and $T_w(x)=T_\infty+Cx^n$ where U_0 and C are constant and *m* and *n* are the velocity and temperature exponent parameter.

The Cartesian coordinates (x, y) and the boundary layer representation on a continuous stretching surface are shown schematically in Figure 3.1. In this figure

the *x*-axis is the direction of the moving surface and *y* –axis is perpendicular to it. The velocity components in the direction of *x* and *y* are *u* and *v* respectively.

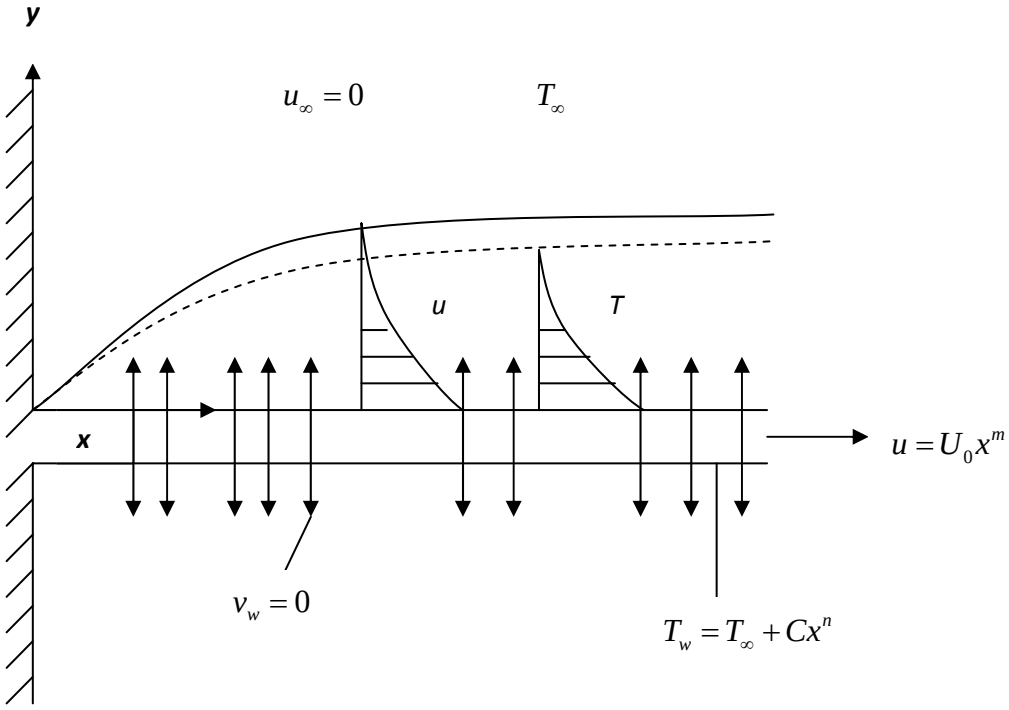

Figure 3.1: Schematic diagram of flow induced by a continuous stretching surface.

Nonsimilar Transformation

In order to solve equations (3.2.1) to (3.2.3), subject to boundary conditions (3.2.4), we use the following similarity transformation (Ali (1994))

$$u = U_0 x^m f'(\eta), \tag{3.2.5 a}$$

$$\eta = y\sqrt{\frac{(m+1)}{2}}\sqrt{\frac{U_0 x^m}{\nu x}}, \tag{3.2.5b}$$

$$v = -\sqrt{\frac{2\nu U_0}{m+1}}x^{\frac{m-1}{2}}\left[\frac{m+1}{2}f + \frac{m-1}{2}f'\eta\right], \tag{3.2.5c}$$

$$T = T_\infty + Cx^n\theta(\eta) \tag{3.2.5d}$$

where η is the similarity variable and *f* is the dimensionless stream function, ψ depends on η only. The stream function ψ is defined as

$$u = \frac{\partial \psi}{\partial y}, \qquad v = -\frac{\partial \psi}{\partial x} \tag{3.2.6}$$

In terms of the stream function ψ, equations (3.2.2) and (3.2.3) become

$$\frac{\partial \psi}{\partial y}\frac{\partial^2 \psi}{\partial x \partial y} - \frac{\partial \psi}{\partial x}\frac{\partial^2 \psi}{\partial y^2} = \nu \frac{\partial^3 \psi}{\partial y^3} \tag{3.2.7}$$

$$\frac{\partial \psi}{\partial y}\frac{\partial T}{\partial x} - \frac{\partial \psi}{\partial x}\frac{\partial T}{\partial y} = \alpha \frac{\partial^2 T}{\partial y^2} \tag{3.2.8}$$

From equations (3.2.5a, b), we obtain the chain rule following system of equations:

$$\frac{\partial^2 \psi}{\partial y^2} = U_0 x^m f'' \sqrt{\frac{(m+1)}{2}} \sqrt{\frac{U_0 x^m}{\nu x}} \tag{3.2.9a}$$

$$\frac{\partial^3 \psi}{\partial y^3} = U_0 x^m f''' (\frac{m+1}{2})(\frac{U_0 x^m}{\nu x}) \tag{3.2.9b}$$

$$\frac{\partial^2 \psi}{\partial x \partial y} = U_0 m x^{m-1} f + U_0 x^m y \sqrt{\frac{(m+1)}{2}} \sqrt{\frac{U_0}{\nu}} \frac{(m-1)}{2x} x^{\frac{m-1}{2}} f' \tag{3.2.9c}$$

From equations (3.2.5c), $T = T_\infty + Cx^n \theta(\eta)$, then

$$\frac{\partial T}{\partial \theta} = Cx^n \theta(\eta) \tag{3.2.10}$$

$$\frac{\partial T}{\partial x} = nCx^{n-1}\theta + Cx^n y \sqrt{\frac{(m+1)}{2}} \sqrt{\frac{U_0}{\nu}} \frac{(m-1)}{2} x^{\frac{m-1}{2}} \theta' \tag{3.2.11a}$$

$$\frac{\partial T}{\partial y} = Cx^n \sqrt{\frac{(m+1)}{2}} \sqrt{\frac{U_0 x^m}{\nu x}} \theta' \tag{3.2.11b}$$

$$\frac{\partial^2 T}{\partial y^2} = Cx^n (\frac{m+1}{2})(\frac{U_0 x^m}{\nu x})\theta'' \tag{3.2.11c}$$

Substituting equations (3.2.9) and (3.2.11) into equations (3.2.7) and (3.2.8), we obtain the following system of equations:

$$f''' + ff'' - \frac{2m}{m+1}(f')^2 = 0, \tag{3.2.12}$$

$$\theta'' + \Pr\left[f\theta' - \frac{2n}{m+1} f'\theta \right] = 0. \tag{3.2.13}$$

subject to

$$f'(0) = 1,\ f(0) = 0, \qquad \theta(0) = 1, \tag{3.2.14}$$

$$f'(\infty) = 0, \qquad \theta(\infty) = 0. \tag{3.2.15}$$

3.3 The Finite Difference Method

To solve (3.2.12) and (3.2.13) using Keller-box method, we write equations (3.2.12) and (3.2.13) as a system of first-order equations. For this purpose, we introduce new dependent variable $u(x, y), v(x, y)$ and $t(x, y)$ and G replaces θ as the variable for temperature. Therefore, we obtain

$$f' = u \qquad u' = v \qquad G' = t \tag{3.3.1a,b,c}$$

$$v' + fv - \frac{2m}{m+1}u^2 = 0 \tag{3.3.1d}$$

$$t' + \Pr\left[ft - \frac{2n}{m+1}uG \right] = 0 \tag{3.3.1e}$$

where the primes denote differentiation with respect to η. In terms of the new dependent variables, the boundary conditions become

$$f(x,0) = 0,\ \ u(x,0) = 1,\ G(x,0) = 1 \tag{3.3.2a}$$

$$u(x,\infty) = 0,\ v(x,\infty) = 0,\ G(x,\infty) = 0 \tag{3.3.2b}$$

The net rectangle considered in the *xy*-plane is shown in Figure 3.1, and the net points are denoted by:

$$x^0 = 0, \qquad x^n = x^{n-1} + k_n, \qquad n = 1, 2, ..., N, \tag{3.3.3a}$$

$$y_0 = 0, \qquad y_j = y_{j-1} + h_j, \qquad j = 1, 2, ..., J, \quad y_J = y_\infty, \tag{3.3.3b}$$

where k_n is the Δx-spacing and h_j is the Δy-spacing. Here *n* and *j* are index points on the *xy*-plane.

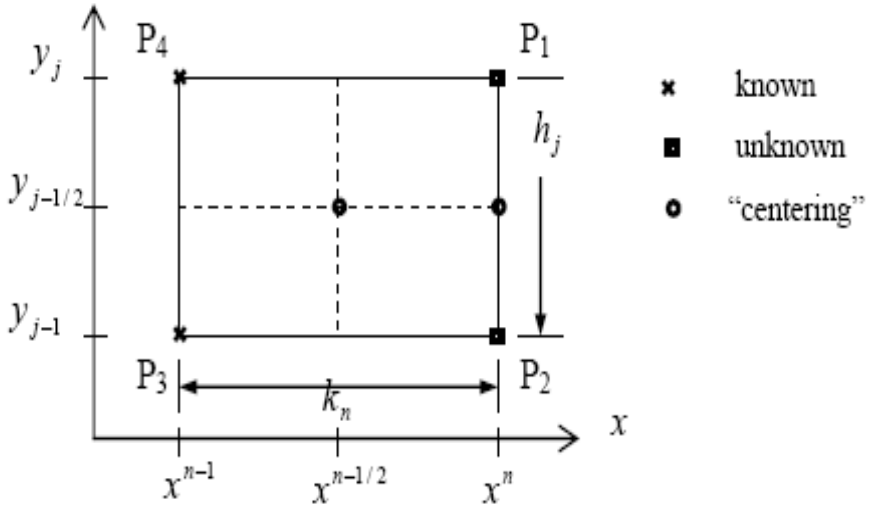

Figure 3.2: Net rectangle for difference approximations

We approximate the quantities (f, u, v, G, t) at points (x^n, y_j) of the net by $(f_j^n, u_j^n, v_j^n, G_j^n, t_j^n)$, which we shall call net functions. We also employ the notation $(\ )_j^n$ for points and quantities midway between net points and for any net function:

$$x^{n-1/2} \equiv \frac{1}{2}(x^n + x^{n-1}), \qquad y_{j-1/2} \equiv \frac{1}{2}(y_j + y_{j-1}) \tag{3.3.4a,b}$$

$$(\ )_j^{n-1/2} = \frac{1}{2}\left[(\ )_j^n + (\ )_j^{n-1}\right] \quad \text{and} \quad (\ )_{j-1/2}^n = \frac{1}{2}\left[(\ )_j^n + (\ )_{j-1}^n\right] \tag{3.3.4c,d}$$

The derivatives in the *x* –direction are written in terms of finite difference as:

$$\frac{\partial(\ )}{\partial x} = \frac{(\ )^n - (\ )^{n-1}}{k_n} \tag{3.3.4e}$$

We write the difference equations that are to approximate equations (3.3.1a) to (3.3.1e) by considering one mesh rectangle as in Figure 3.1. We start by writing the finite difference approximations of the ordinary differential equations (3.3.1a) to (3.3.1c) for the midpoint $\left(x^n, y_{j-1/2}\right)$ of the segment $\mathrm{P_1P_2}$, using centered difference derivatives. This process is called "centering about $\left(x^n, y_{j-1/2}\right)$". We get

$$\frac{\left(f_j^n - f_{j-1}^n\right)}{h_j} = \frac{1}{2}\left(u_j^n + u_{j-1}^n\right) = u_{j-1/2}^n, \tag{3.3.5a}$$

$$\frac{\left(u_j^n - u_{j-1}^n\right)}{h_j} = \frac{1}{2}\left(v_j^n + v_{j-1}^n\right) = v_{j-1/2}^n, \tag{3.3.5b}$$

$$\frac{\left(G_j^n - G_{j-1}^n\right)}{h_j} = \frac{1}{2}\left(t_j^n + t_{j-1}^n\right) = t_{j-1/2}^n, \tag{3.3.5c}$$

Equations (3.3.1d,e) are approximated by centering the midpoint $\left(x^{n-1/2}, y_{j-1/2}\right)$ of the rectangle $\mathrm{P_1P_2P_3P_4}$. This can be done in two steps. In the first step, we center equations (3.3.1d,e) about the point $\left(x^{n-1/2}, y\right)$ without specifying *y*. We denote the left-hand side of equations (3.3.1d,e) by L_1 and L_2, then the approximations are

$$\frac{1}{2}\left(L_1^n + L_1^{n-1}\right) = 0, \tag{3.3.6a}$$

$$\frac{1}{2}\left(L_2^n + L_2^{n-1}\right) = 0, \tag{3.3.6b}$$

Rearranging equation (3.3.6) and using equation (3.3.4c), the difference approximation to equations (3.3.1d,e) at $x^{n-1/2}$ become

$$\left(v'\right)^n + \left(fv\right)^n - \frac{2m}{m+1}\left(u^2\right)^n = -\left[L_1\right]^{n-1}, \tag{3.3.7a}$$

$$\left(t'\right)^n + \mathrm{Pr}\left[\left(ft\right)^n - \frac{2n}{m+1}\left(uG\right)^n\right] = -\left[L_2\right]^{n-1}, \tag{3.3.7b}$$

where

$$L_1^{n-1} = \left[v' + fv - \frac{2m}{m+1} u^2 \right], \tag{3.3.8a}$$

$$L_2^{n-1} = \left[t' + \Pr\left[ft - \frac{2n}{m+1} uG \right] \right], \tag{3.3.8b}$$

where the identity sign introduces useful shorthand: $[\ ]^{n-1}$ means that the quantities in square bracket are evaluated at $x = x^{n-1}$.

The second step we center equations (3.3.7) about point $\left(x^{n-1/2}, y_{j-1/2}\right)$ by using equation (3.3.4d) and we get

$$\frac{\left(v_j^n - v_{j-1}^n\right)}{h_j} + f_{j-1/2}^n v_{j-1/2}^n - \frac{2m}{m+1}\left(u_{j-1/2}^n\right)^2 = \left[-L_1\right]_{j-1/2}^{n-1}, \tag{3.3.9a}$$

$$\frac{\left(t_j^n - t_{j-1}^n\right)}{h_j} + \Pr\left[f_{j-1/2}^n t_{j-1/2}^n - \frac{2n}{m+1} u_{j-1/2}^n G_{j-1/2}^n \right] = \left[-L_2\right]_{j-1/2}^{n-1}, \tag{3.3.9b}$$

where

$$\left[L_1\right]_{j-1/2}^{n-1} = \left[\frac{\left(v_j - v_{j-1}\right)}{h_j} + f_{j-1/2} v_{j-1/2} - \left(u_{j-1/2}\right)^2 \right]^{n-1},$$

$$\left[L_2\right]_{j-1/2}^{n-1} = \frac{\left(t_j - t_{j-1}\right)}{h_j} + \Pr\left[f_{j-1/2} t_{j-1/2} - u_{j-1/2} G_{j-1/2} \right]^{n-1},$$

Equations (3.3.5) and (3.3.9) are imposed for $j = 1, 2, ..., J$ at given *n*, and the transformed boundary layer thickness, y_J, is to be sufficiently large so that it is beyond to the edge of the boundary layer by Keller and Cebeci (1972).

At $x = x^n$, the boundary conditions (3.3.2) become

$$f_0^n = 0, \quad u_0^n = 1, \quad G_0^n = 1, \quad u_j^n = 0, \quad v_j^n = 0, \quad G_j^n = 0 \tag{3.3.10}$$

3.4 Newton's Method

If we assume $f_j^{n-1}, u_j^{n-1}, v_j^{n-1}, G_j^{n-1}, t_j^{n-1}$ to be known for $0 \le j \le J$, then equations (3.3.5), (3.3.9) and (3.3.10) are a system of equations for the solution of the unknowns $\left(f_j^n, u_j^n, v_j^n, G_j^n, t_j^n \right)$, $j = 0, 1, ..., J$. For simplicity of notation we shall write the unknowns at $x = x^n$ as

$$\left(f_j^n, u_j^n, v_j^n, G_j^n, t_j^n \right) = \left(f_j, u_j, v_j, G_j, t_j \right)$$

Then the system of equations (3.3.5) and (3.3.9) can be written as

$$f_j - f_{j-1} - \frac{h_j}{2}\left(u_j + u_{j-1} \right) = 0, \tag{3.4.1a}$$

$$u_j - u_{j-1} - \frac{h_j}{2}\left(v_j + v_{j-1} \right) = 0, \tag{3.4.1b}$$

$$G_j - G_{j-1} - \frac{h_j}{2}\left(t_j + t_{j-1} \right) = 0, \tag{3.4.1c}$$

$$\left(v_j - v_{j-1} \right) + \frac{h_j}{4}\left(f_j + f_{j-1} \right)\left(v_j + v_{j-1} \right) - \frac{2m}{m+1}\left(\frac{h_j}{4} \right)\left(u_j + u_{j-1} \right)^2 = \left(R_1 \right)_{j-1/2}^{n-1}, \tag{3.41d}$$

$$\begin{aligned} &\left(t_j - t_{j-1} \right) + \Pr\left[\frac{h_j}{4}\left(f_j + f_{j-1} \right)\left(t_j + t_{j-1} \right) \right] \\ &- \Pr\left[\frac{2n}{m+1}\left(\frac{h_j}{4} \right)\left(u_j + u_{j-1} \right)\left(G_j + G_{j-1} \right) \right] = \left(R_2 \right)_{j-1/2}^{n-1} \end{aligned} \tag{3.4.1e}$$

where

$$\left(R_1 \right)_{j-1/2}^{n-1} = h_j \left[\frac{\left(v_j - v_{j-1} \right)}{h_j} + f_{j-1/2} v_{j-1/2} - \frac{2m}{m+1}\left(u_{j-1/2} \right)^2 \right]^{n-1}, \tag{3.4.2a}$$

$$\left(R_2\right)_{j-1/2}^{n-1} = -h_j\left[\frac{\left(t_j - t_{j-1}\right)}{h_j} + \Pr\left[f_{j-1/2}t_{j-1/2} - \frac{2n}{m+1}u_{j-1/2}G_{j-1/2}\right]\right]^{n-1}, \qquad (3.4.2b)$$

$\left(R_1\right)_{j-1/2}^{n-1}$ and $\left(R_2\right)_{j-1/2}^{n-1}$ involves only known quantities if we assume that the solution is known on $x = x^{n-1}$. To solve equation (3.4.1) with (3.3.10) by Newton's method, we introduce the iterates $\left[f_j^{(i)}, u_j^{(i)}, v_j^{(i)}, G_j^{(i)}, t_j^{(i)}\right],\ \ i = 0,1,2,\ldots.$

In order to linearize the nonlinear system of equations (3.4.1) using Newton's method, we introduce the following iterates

$$\begin{aligned} &f_j^{(i+1)} = f_j^{(i)} + \delta f_j^{(i)}, \quad u_j^{(i+1)} = u_j^{(i)} + \delta u_j^{(i)}, \quad v_j^{(i+1)} = v_j^{(i)} + \delta v_j^{(i)} \\ &G_j^{(i+1)} = G_j^{(i)} + \delta G_j^{(i)}, \quad t_j^{(i+1)} = t_j^{(i)} + \delta t_j^{(i)}. \end{aligned} \qquad (3.4.3)$$

Then we substitute (3.4.3) into (3.4.1) except the term on x^{n-1}, we get

$$\left(f_j^{(i)} + \delta f_j^{(i)}\right) - \left(f_{j-1}^{(i)} + \delta f_{j-1}^{(i)}\right) - \frac{h_j}{2}\left(u_j^{(i)} + \delta u_j^{(i)} + u_{j-1}^{(i)} + \delta u_{j-1}^{(i)}\right) = 0,$$

$$\left(u_j^{(i)} + \delta u_j^{(i)}\right) - \left(u_{j-1}^{(i)} + \delta u_{j-1}^{(i)}\right) - \frac{h_j}{2}\left(v_j^{(i)} + \delta v_j^{(i)} + v_{j-1}^{(i)} + \delta v_{j-1}^{(i)}\right) = 0,$$

$$\left(G_j^{(i)} + \delta G_j^{(i)}\right) - \left(G_{j-1}^{(i)} + \delta G_{j-1}^{(i)}\right) - \frac{h_j}{2}\left(t_j^{(i)} + \delta t_j^{(i)} + t_{j-1}^{(i)} + \delta t_{j-1}^{(i)}\right) = 0,$$

$$\left(v_j^{(i)} + \delta v_j^{(i)}\right) - \left(v_{j-1}^{(i)} + \delta v_{j-1}^{(i)}\right) + \frac{h_j}{4}\left(f_j^{(i)} + \delta f_j^{(i)} + f_{j-1}^{(i)} + \delta f_{j-1}^{(i)}\right)\left(v_j^{(i)} + \delta v_j^{(i)} + v_{j-1}^{(i)} + \delta v_{j-1}^{(i)}\right)$$
$$-\frac{2m}{m+1}\left(\frac{h_j}{4}\right)\left(u_j^{(i)} + \delta u_j^{(i)} + u_{j-1}^{(i)} + \delta u_{j-1}^{(i)}\right)^2 = \left(R_1\right)_{j-1/2}^{n-1},$$

$$\left(t_j^{(i)} + \delta t_j^{(i)}\right) - \left(t_{j-1}^{(i)} + \delta t_{j-1}^{(i)}\right) + \Pr\left[\frac{h_j}{4}\left(f_j^{(i)} + \delta f_j^{(i)} + f_{j-1}^{(i)} + \delta f_{j-1}^{(i)}\right)\left(t_j^{(i)} + \delta t_j^{(i)} + t_{j-1}^{(i)} + \delta t_{j-1}^{(i)}\right)\right]$$
$$-\Pr\left[\frac{2n}{m+1}\left(\frac{h_j}{4}\right)\left(u_j^{(i)} + \delta u_j^{(i)} + u_{j-1}^{(i)} + \delta u_{j-1}^{(i)}\right)\left(G_j^{(i)} + \delta G_j^{(i)} + G_{j-1}^{(i)} + \delta G_{j-1}^{(i)}\right)\right] = \left(R_2\right)_{j-1/2}^{n-1},$$

Next we drop the terms that are quadratic in $\left(\delta f_j^{(i)}, \delta u_j^{(i)}, \delta v_j^{(i)}, \delta G_j^{(i)}, \delta t_j^{(i)}\right)$ and we have also drop the superscript *I* for simplicity. After some algebraic manipulations, the following linear tridiagonal system of equations is obtained

$$\delta f_j - \delta f_{j-1} - \frac{1}{2} h_j \left(\delta u_j + \delta u_{j-1}\right) = \left(r_1\right)_{j-1/2}, \tag{3.4.4a}$$

$$\delta u_j - \delta u_{j-1} - \frac{1}{2} h_j \left(\delta v_j + \delta v_{j-1}\right) = \left(r_2\right)_{j-1/2}, \tag{3.4.4b}$$

$$\delta G_j - \delta G_{j-1} - \frac{1}{2} h_j \left(\delta t_j + \delta t_{j-1}\right) = \left(r_3\right)_{j-1/2}, \tag{3.4.4c}$$

$$\begin{aligned}&\left(a_1\right)_j \delta v_j + \left(a_2\right)_j \delta v_{j-1} + \left(a_3\right)_j \delta f_j + \left(a_4\right)_j \delta f_{j-1} + \left(a_5\right)_j \delta u_j \\ &+ \left(a_6\right)_j \delta u_{j-1} = \left(r_4\right)_{j-1/2},\end{aligned} \tag{3.4.4d}$$

$$\begin{aligned}&\left(b_1\right)_j \delta t_j + \left(b_2\right)_j \delta t_{j-1} + \left(b_3\right)_j \delta f_j + \left(b_4\right)_j \delta f_{j-1} + \left(b_5\right)_j \delta u_j \\ &+ \left(b_6\right)_j \delta u_{j-1} + \left(b_7\right)_j \delta G_j + \left(b_8\right)_j \delta G_{j-1} = \left(r_5\right)_{j-1/2},\end{aligned} \tag{3.4.4e}$$

where

$$\begin{aligned}&\left(a_1\right)_j = 1 + \frac{h_j}{2} f_{j-1/2}, \\ &\left(a_2\right)_j = -1 + \frac{h_j}{2} f_{j-1/2} = \left(a_1\right)_j - 2, \\ &\left(a_3\right)_j = \frac{h_j}{2} v_{j-1/2}, \qquad \left(a_4\right)_j = \left(a_3\right)_j, \\ &\left(a_5\right)_j = -\frac{2m}{m+1} h_j u_{j-1/2}, \qquad \left(a_6\right)_j = \left(a_5\right)_j,\end{aligned} \tag{3.4.5}$$

$$\begin{aligned}&\left(b_1\right)_j = 1 + \frac{\mathrm{Pr}}{2} h_j f_{j-1/2}, \\ &\left(b_2\right)_j = -1 + \frac{\mathrm{Pr}}{2} h_j f_{j-1/2} = \left(b_1\right)_j - 2, \\ &\left(b_3\right)_j = \frac{\mathrm{Pr}}{2} h_j t_{j-1/2}, \qquad \left(b_4\right)_j = \left(b_3\right)_j, \\ &\left(b_5\right)_j = -\left(\frac{n}{m+1}\right) \mathrm{Pr}\, h_j G_{j-1/2}, \qquad \left(b_6\right)_j = \left(b_5\right)_j,\end{aligned} \tag{3.4.6}$$

$$(b_7)_j = -\left(\frac{n}{m+1}\right)\Pr h_j u_{j-1/2}, \qquad (b_8)_j = (b_7)_j,$$

$$\begin{aligned}
(r_1)_{j-1/2} &= f_{j-1} - f_j + h_j u_{j-1/2},\\
(r_2)_{j-1/2} &= u_{j-1} - u_j + h_j v_{j-1/2},\\
(r_3)_{j-1/2} &= G_{j-1} - G_j + h_j t_{j-1/2},\\
(r_4)_j &= (v_{j-1} - v_j) - h_j\left(-f_{j-1/2} v_{j-1/2} + \frac{2m}{m+1} u_{j-1/2}^2\right),\\
(r_5)_j &= (t_{j-1} - t_j) - \Pr h_j\left(-f_{j-1/2} t_{j-1/2} + \frac{2n}{m+1} u_{j-1/2} G_{j-1/2}\right),
\end{aligned} \tag{3.4.7}$$

To complete the system (3.4.4), we recall the boundary condition (3.3.10), which can be satisfied exactly with no iteration. So, to maintain these correct values in all the iterates, we take

$$\delta f_0 = 0, \quad \delta u_0 = 0, \quad \delta G_0 = 0, \quad \delta u_J = 0, \quad \delta v_J = 0, \quad \delta G_J = 0 \tag{3.4.8}$$

3.5 Block-elimination Method

The linear system (3.4.4) can be solved by the block-elimination method. The linearized difference equations of the system (3.4.4) have a block-tridiagonal structure.

Generally, the block-tridiagonal structure consists of variable or constant, but here, an interesting feature can be observed that is, for the Keller-box method it consists of block matrices. Before we solved the linear system (3.4.4) using block-elimination method, we will show how to get the elements of the block matrices from the linear system (3.4.4). We consider three cases, namely when $j = 1, J-1$ and J.

When $j = 1$, the linear system (3.4.4) become

$$\delta f_1 - \delta f_0 - \frac{1}{2} h_1 \left(\delta u_1 + \delta u_0 \right) = \left(r_1 \right)_{1-(1/2)},$$

$$\delta u_1 - \delta u_0 - \frac{1}{2} h_1 \left(\delta v_1 + \delta v_0 \right) = \left(r_2 \right)_{1-(1/2)},$$

$$\delta G_1 - \delta G_0 - \frac{1}{2} h_1 \left(\delta t_1 + \delta t_0 \right) = \left(r_3 \right)_{1-(1/2)},$$

$$\left(a_1 \right)_1 \delta v_1 + \left(a_2 \right)_1 \delta v_0 + \left(a_3 \right)_1 \delta f_1 + \left(a_4 \right)_1 \delta f_0 + \left(a_5 \right)_1 \delta u_1 + \left(a_6 \right)_1 \delta u_0 = \left(r_4 \right)_{1-(1/2)},$$

$$\left(b_1 \right)_1 \delta t_1 + \left(b_2 \right)_1 \delta t_0 + \left(b_3 \right)_1 \delta f_1 + \left(b_4 \right)_1 \delta f_0 + \left(b_5 \right)_1 \delta u_1 + \left(b_6 \right)_1 \delta u_0 + \left(b_7 \right)_1 \delta G_1 + \left(b_8 \right)_1 \delta G_0 = \left(r_5 \right)_{1-(1/2)},$$

The corresponding matrix form is [we let $d_1 = -\frac{1}{2} h_1$, and $\delta f_0 = 0,\ \delta u_0 = 0,\ \delta G_0 = 0$] from (3.4.8):

$$\begin{bmatrix} 0 & 0 & 1 & 0 & 0 \\ d_1 & 0 & 0 & d_1 & 0 \\ 0 & d_1 & 0 & 0 & d_1 \\ \left(a_2 \right)_1 & 0 & \left(a_3 \right)_1 & \left(a_1 \right)_1 & 0 \\ 0 & \left(b_2 \right)_1 & \left(b_3 \right)_1 & 0 & \left(b_1 \right)_1 \end{bmatrix} \begin{bmatrix} \delta v_0 \\ \delta t_0 \\ \delta f_1 \\ \delta v_1 \\ \delta t_1 \end{bmatrix} +$$

$$\begin{bmatrix} d_1 & 0 & 0 & 0 & 0 \\ 1 & 0 & 0 & 0 & 0 \\ 0 & 1 & 0 & 0 & 0 \\ \left(a_5 \right)_1 & 0 & 0 & 0 & 0 \\ \left(b_5 \right)_1 & \left(b_7 \right)_1 & 0 & 0 & 0 \end{bmatrix} \begin{bmatrix} \delta u_1 \\ \delta G_1 \\ \delta f_2 \\ \delta v_2 \\ \delta t_2 \end{bmatrix} = \begin{bmatrix} \left(r_1 \right)_{1-(1/2)} \\ \left(r_2 \right)_{1-(1/2)} \\ \left(r_3 \right)_{1-(1/2)} \\ \left(r_4 \right)_{1-(1/2)} \\ \left(r_5 \right)_{1-(1/2)} \end{bmatrix}$$

For the value of $j = 1$, we have $\left[A_1 \right]\left[\delta_1 \right] + \left[C_1 \right]\left[\delta_2 \right] = \left[r_1 \right]$

When $j = J - 1$, the linear system (3.4.4) become

$$\delta f_{J-1} - \delta f_{J-2} - \frac{1}{2} h_{J-1} \left(\delta u_{J-1} + \delta u_{J-2} \right) = \left(r_1 \right)_{(J-1)-(1/2)},$$

$$\delta u_{J-1} - \delta u_{J-2} - \frac{1}{2} h_{J-1} \left(\delta v_{J-1} + \delta v_{J-2} \right) = \left(r_2 \right)_{(J-1)-(1/2)},$$

$$\delta G_{J-1} - \delta G_{J-2} - \frac{1}{2} h_{J-1} \left(\delta t_{J-1} + \delta t_{J-2} \right) = \left(r_3 \right)_{(J-1)-(1/2)},$$

$$\left(a_1 \right)_{J-1} \delta v_{J-1} + \left(a_2 \right)_{J-1} \delta v_{J-2} + \left(a_3 \right)_{J-1} \delta f_{J-1} + \left(a_4 \right)_{J-1} \delta f_{J-2} + \left(a_5 \right)_{J-1} \delta u_{J-1}$$
$$+ \left(a_6 \right)_{J-1} \delta u_{J-2} = \left(r_4 \right)_{(J-1)-(1/2)},$$

$$\left(b_1 \right)_{J-1} \delta t_{J-1} + \left(b_2 \right)_{J-1} \delta t_{J-2} + \left(b_3 \right)_{J-1} \delta f_{J-1} + \left(b_4 \right)_{J-1} \delta f_{J-2} + \left(b_5 \right)_{J-1} \delta u_{J-1}$$
$$+ \left(b_6 \right)_{J-1} \delta u_{J-2} + \left(b_7 \right)_{J-1} \delta G_{J-1} + \left(b_8 \right)_{J-1} \delta G_{J-2} = \left(r_5 \right)_{(J-1)-(1/2)},$$

The corresponding matrix form is (we let $d_{J-1} = -\frac{1}{2} h_{J-1}$)

$$\begin{bmatrix} 0 & 0 & -1 & 0 & 0 \\ 0 & 0 & 0 & d_{J-1} & 0 \\ 0 & 0 & 0 & 0 & d_{J-1} \\ 0 & 0 & \left(a_4 \right)_{J-1} & \left(a_2 \right)_{J-1} & 0 \\ 0 & 0 & \left(b_4 \right)_{J-1} & 0 & \left(b_2 \right)_{J-1} \end{bmatrix} \begin{bmatrix} \delta u_{J-3} \\ \delta G_{J-3} \\ \delta f_{J-2} \\ \delta v_{J-2} \\ \delta t_{J-2} \end{bmatrix} +$$

$$\begin{bmatrix} d_{J-1} & 0 & 1 & 0 & 0 \\ -1 & 0 & 0 & d_{J-1} & 0 \\ 0 & -1 & 0 & 0 & d_{J-1} \\ \left(a_6 \right)_{J-1} & 0 & \left(a_3 \right)_{J-1} & \left(a_1 \right)_{J-1} & 0 \\ \left(b_6 \right)_{J-1} & \left(b_8 \right)_{J-1} & \left(b_3 \right)_{J-1} & 0 & \left(b_1 \right)_{J-1} \end{bmatrix} \begin{bmatrix} \delta u_{J-2} \\ \delta G_{J-2} \\ \delta f_{J-1} \\ \delta v_{J-1} \\ \delta t_{J-1} \end{bmatrix} +$$

$$\begin{bmatrix} d_{J-1} & 0 & 0 & 0 & 0 \\ 1 & 0 & 0 & 0 & 0 \\ 0 & 1 & 0 & 0 & 0 \\ \left(a_5 \right)_{J-1} & 0 & 0 & 0 & 0 \\ \left(b_5 \right)_{J-1} & \left(b_7 \right)_{J-1} & 0 & 0 & 0 \end{bmatrix} \begin{bmatrix} \delta u_{J-1} \\ \delta G_{J-1} \\ \delta f_J \\ \delta v_J \\ \delta t_J \end{bmatrix} = \begin{bmatrix} \left(r_1 \right)_{1-(1/2)} \\ \left(r_2 \right)_{1-(1/2)} \\ \left(r_3 \right)_{1-(1/2)} \\ \left(r_4 \right)_{1-(1/2)} \\ \left(r_5 \right)_{1-(1/2)} \end{bmatrix}$$

For all values of $j = 2, 3, ..., J-1,$ we have

$$\left[B_j \right] \left[\delta_{j-1} \right] + \left[A_j \right] \left[\delta_j \right] + \left[C_j \right] \left[\delta_{j+1} \right] = \left[r_j \right]$$

Finally, when $j = J$, the linear system (3.4.4) become

$$\delta f_J - \delta f_{J-1} - \frac{1}{2} h_J \left(\delta u_J + \delta u_{J-1}\right) = \left(r_1\right)_{J-(1/2)},$$

$$\delta u_J - \delta u_{J-1} - \frac{1}{2} h_J \left(\delta v_J + \delta v_{J-1}\right) = \left(r_2\right)_{J-(1/2)},$$

$$\delta G_J - \delta G_{J-1} - \frac{1}{2} h_J \left(\delta t_J + \delta t_{J-1}\right) = \left(r_3\right)_{J-(1/2)},$$

$$\left(a_1\right)_J \delta v_J + \left(a_2\right)_J \delta v_{J-1} + \left(a_3\right)_J \delta f_J + \left(a_4\right)_J \delta f_{J-1} + \left(a_5\right)_J \delta u_J + \left(a_6\right)_J \delta u_{J-1} = \left(r_4\right)_{J-(1/2)},$$

$$\left(b_1\right)_J \delta t_J + \left(b_2\right)_J \delta t_{J-1} + \left(b_3\right)_J \delta f_J + \left(b_4\right)_J \delta f_{J-1} + \left(b_5\right)_J \delta u_J + \left(b_6\right)_J \delta u_{J-1} + \left(b_7\right)_J \delta G_J + \left(b_8\right)_J \delta G_{J-1} = \left(r_5\right)_{J-(1/2)},$$

The corresponding matrix form is (we let $d_J = -\frac{1}{2} h_J$, and $\delta u_J = 0$, $\delta G_J = 0$ from (3.4.8)):

$$\begin{bmatrix} 0 & 0 & -1 & 0 & 0 \\ 0 & 0 & 0 & d_J & 0 \\ 0 & 0 & 0 & 0 & d_J \\ 0 & 0 & \left(a_4\right)_J & \left(a_2\right)_J & 0 \\ 0 & 0 & \left(b_4\right)_J & 0 & \left(b_2\right)_J \end{bmatrix} \begin{bmatrix} \delta u_{J-2} \\ \delta G_{J-2} \\ \delta f_{J-1} \\ \delta v_{J-1} \\ \delta t_{J-1} \end{bmatrix} +$$

$$\begin{bmatrix} d_J & 0 & 1 & 0 & 0 \\ -1 & 0 & 0 & d_J & 0 \\ 0 & -1 & 0 & 0 & d_J \\ \left(a_6\right)_J & 0 & \left(a_3\right)_J & \left(a_1\right)_J & 0 \\ \left(b_6\right)_J & \left(b_8\right)_J & \left(b_3\right)_J & 0 & \left(b_1\right)_J \end{bmatrix} \begin{bmatrix} \delta u_{J-1} \\ \delta G_{J-1} \\ \delta f_J \\ \delta v_J \\ \delta t_J \end{bmatrix} = \begin{bmatrix} \left(r_1\right)_{J-(1/2)} \\ \left(r_2\right)_{J-(1/2)} \\ \left(r_3\right)_{J-(1/2)} \\ \left(r_4\right)_{J-(1/2)} \\ \left(r_5\right)_{J-(1/2)} \end{bmatrix}$$

For all values of $j = J$, we have $\left[B_j\right]\left[\delta_{j-1}\right] + \left[A_j\right]\left[\delta_j\right] = \left[r_j\right]$

Therefore, for $j = 1, 2, 3, ..., J-1, J$, we have

$$
\begin{aligned}
&j=1: && [A_1][\delta_1]+[C_1][\delta_2]=[r_1]\\
&j=2: && [B_2][\delta_1]+[A_2][\delta_2]+[C_2][\delta_3]=[r_2]\\
&j=3: && [B_3][\delta_2]+[A_3][\delta_3]+[C_3][\delta_4]=[r_3]\\
&\ \vdots && \qquad\qquad\ \vdots\\
&j=J-1: && [B_{J-1}][\delta_{J-2}]+[A_{J-1}][\delta_{J-1}]+[C_{J-1}][\delta_J]=[r_{J-1}]\\
&j=J: && [B_J][\delta_{J-1}]+[A_J][\delta_J]=[r_J]
\end{aligned}
$$

In the matrix form, this can be written as

$$\boldsymbol{A}\delta=\boldsymbol{r} \tag{3.5.1}$$

where

$$
\boldsymbol{A}=\begin{bmatrix}
[A_1] & [C_1] & & & \\
[B_2] & [A_2] & [C_2] & & \\
 & \ddots & \ddots & \ddots & \\
 & & [B_{J-1}] & [A_{J-1}] & [C_{J-1}]\\
 & & & [B_J] & [A_J]
\end{bmatrix},\ \delta=\begin{bmatrix}
[\delta_1]\\ [\delta_2]\\ \vdots\\ [\delta_{J-1}]\\ [\delta_J]
\end{bmatrix},\ \boldsymbol{r}=\begin{bmatrix}
[r_1]\\ [r_2]\\ \vdots\\ [r_{J-1}]\\ [r_J]
\end{bmatrix}
$$

The elements of the matrices are as follows

$$
[A_1]=\begin{bmatrix}
0 & 0 & 1 & 0 & 0\\
d_1 & 0 & 0 & d_1 & 0\\
0 & d_1 & 0 & 0 & d_1\\
(a_2)_1 & 0 & (a_3)_1 & (a_1)_1 & 0\\
0 & (b_2)_1 & (b_3)_1 & 0 & (b_1)_1
\end{bmatrix}, \tag{3.5.2a}
$$

$$
[A_j]=\begin{bmatrix}
d_j & 0 & 1 & 0 & 0\\
-1 & 0 & 0 & d_j & 0\\
0 & -1 & 0 & 0 & d_j\\
(a_6)_j & 0 & (a_3)_j & (a_1)_j & 0\\
(b_6)_j & (b_8)_j & (b_3)_j & 0 & (b_1)_j
\end{bmatrix},\ 2\le j\le J \tag{3.5.2b}
$$

$$\left[B_j\right]=\begin{bmatrix} 0 & 0 & -1 & 0 & 0 \\ 0 & 0 & 0 & d_j & 0 \\ 0 & 0 & 0 & 0 & d_j \\ 0 & 0 & (a_4)_j & (a_2)_j & 0 \\ 0 & 0 & (b_4)_j & 0 & (b_2)_j \end{bmatrix},\ 2 \le j \le J \tag{3.5.3}$$

$$\left[C_j\right]=\begin{bmatrix} d_j & 0 & 0 & 0 & 0 \\ 1 & 0 & 0 & 0 & 0 \\ 0 & 1 & 0 & 0 & 0 \\ (a_5)_j & 0 & 0 & 0 & 0 \\ (b_5)_j & (b_7)_j & 0 & 0 & 0 \end{bmatrix},\ 1 \le j \le J-1 \tag{3.5.4}$$

$$\left[\delta_1\right]=\begin{bmatrix} \delta v_0 \\ \delta t_0 \\ \delta f_1 \\ \delta v_1 \\ \delta t_1 \end{bmatrix}, \qquad \delta=\begin{bmatrix} \delta u_{j-1} \\ \delta G_{j-1} \\ \delta f_j \\ \delta v_j \\ \delta t_j \end{bmatrix}, \quad 2 \le j \le J \tag{3.5.5a, b}$$

And $$\left[r_j\right]=\begin{bmatrix} (r_1)_{j-(1/2)} \\ (r_2)_{j-(1/2)} \\ (r_3)_{j-(1/2)} \\ (r_4)_{j-(1/2)} \\ (r_5)_{j-(1/2)} \end{bmatrix},\ 1 \le j \le J \tag{3.5.6}$$

The coefficient matrix $\boldsymbol{A}$ is known as tridiagonal matrix due to the fact that all elements of $\boldsymbol{A}$ are zero except those on the three main diagonal. To solve equation (3.5.1), according to the block elimination method as described in Cebeci and Bradshaw (1988), we assume matrix $\boldsymbol{A}$ is nonsingular and we seek a factorization of the form

$$\boldsymbol{A}=\boldsymbol{LU} \tag{3.5.7}$$

where

$$\boldsymbol{L}=\begin{bmatrix}[\alpha_1] & & & & & & \\ [B_2] & [\alpha_2] & & & & & \\ & [B_3] & [\alpha_3] & & & & \\ & & \ddots & & & & \\ & & & \ddots & & & \\ & & & & [B_{J-1}] & [\alpha_{J-1}] & \\ & & & & & [B_J] & [\alpha_J]\end{bmatrix}$$

and

$$\boldsymbol{U}=\begin{bmatrix}[I] & [\Gamma_1] & & & & & \\ & [I] & [\Gamma_2] & & & & \\ & & [I] & [\Gamma_3] & & & \\ & & & \ddots & & & \\ & & & \ddots & & & \\ & & & & & [I] & [\Gamma_{J-1}] \\ & & & & & & [I]\end{bmatrix},$$

$[I]$ is the identity matrix of order 5. $[\alpha_i]$ and $[\Gamma_i]$ are 5 x 5 matrices whose element are determined by the following equations:

$$[\alpha_1]=[A_1], \tag{3.5.8a}$$

$$[A_1][\Gamma_1]=[C_1] \tag{3.5.8b}$$

and

$$[\alpha_j]=[A_j]-[B_j][\Gamma_{j-1}], \qquad j=2,3,\ldots,J \tag{3.5.8c}$$

$$[\alpha_j][\Gamma_j]=[C_j], \qquad j=2,3,\ldots,J-1. \tag{3.5.8d}$$

By substituting (3.5.7) into (3.5.1), we get

$$\boldsymbol{LU}\delta=\boldsymbol{r} \tag{3.5.9}$$

If we define $$\boldsymbol{U}\delta=\boldsymbol{W} \tag{3.5.10}$$

then equation (3.5.9) becomes $\boldsymbol{LW} = \boldsymbol{r}$ (3.5.11)

where

$$\boldsymbol{W} = \begin{bmatrix} [W_1] \\ [W_2] \\ \vdots \\ [W_{J-1}] \\ [W_J] \end{bmatrix},$$

and $[W_j]$ are 5 x 1 column matrices. The elements $\boldsymbol{W}$ can be solved from equation (3.5.11):

$$[\alpha_1][W_1] = [r_1], \tag{3.5.12a}$$

$$[\alpha_j][W_j] = [r_j] - [B_j][W_{j-1}], \qquad 2 \le j \le J \tag{3.5.12b}$$

The solution of equation (3.5.7) by block-elimination method consists of two sweeps. The step in which Γ_j, α_j and W_j are calculated, is usually referred to as the *forward sweep*. They are computed from the recursion formulas given by (3.5.8) and (3.5.12). When the elements of $\boldsymbol{W}$ are found, equation (3.5.10) then gives the solution of δ in the so called *backward sweep*, in which the elements are obtained by the following relations:

$$[\delta_J] = [W_J], \tag{3.5.13a}$$

$$[\delta_j] = [W_j] - [\Gamma_j][\delta_{j+1}], \qquad 1 \le j \le J-1 \tag{3.5.13b}$$

Once the elements of δ are found, equation (3.4.4) can be used to find (i+1)th iteration in equation (3.4.3).

These calculations are repeated until some convergence criterion is satisfied. In laminar boundary layer calculations, the wall shear stress parameter $v(x,0)$ is

usually used as the convergence criterion. This is probably because in boundary layer calculations, it is find that the greatest error usually appears in the wall shear stress parameter. Calculations are stopped when

$$\left|\delta v_0^{(i)}\right| < \varepsilon_1 \tag{3.5.14}$$

where ε_1 is a small prescribed value.

In this study, we consider $\varepsilon_1 = 10^{-5}$ that gives about four decimal places accuracy for most predicted quantities (Cebeci and Bradshaw (1988)).

3.6 Starting Conditions

In the numerical computation, a proper step size Δy and an appropriate y_∞ value (an approximate to $y = \infty$) must be determined. All of these value usually determined by a trial and error approach (Chen (1998)). In general, if the appropriate y_∞ value at a given x is not known, the computation can be started by using small value of y_∞ and the successively increase the values of y_∞ until a suitable y_∞ is obtained.

For most laminar boundary layer flows the transformed boundary layer thickness $y_\infty(x)$ is almost constant. The value of y_∞ typically lies between 5 and 10. Once we obtain the proper values of y_∞, a reasonable choice of step size Δy and Δx should be determined. In most laminar boundary layer flows, a step size $\Delta y = 0.02$ to 0.04 is sufficient to provide accurate and comparable results.

In order to start and proceed with the numerical computation, it is necessary to make initial guesses for the function f, u, v, G and t across the boundary layer. To start a solution at a given x, it is necessary to assume distribution curves for the

velocity, u and the temperature, G between $y = 0$ and $y = y_\infty$. We used the distribution curves given by Bejan (1984) and Ghoshdastidar (2004). These are used as the initial guess because both the velocity and temperature profiles satisfy the boundary condition for the problem of heat transfer characteristic of a continuous stretching surface with thermal boundary condition for uniform and variable surface temperature.

The velocity profile chosen is

$$u = f' = \left(1 - \frac{y}{y_\infty}\right)^2 \tag{3.6.1}$$

and the temperature profile is

$$G = \theta = \left(1 - \frac{y}{y_\infty}\right)^2 \tag{3.6.2}$$

Therefore, integrating and differentiating equation (3.6.1) with respect to *y*, we get the following expression for *f* and *v*

$$f = \int_{y=0}^{y=y_\infty} u dy = y - \frac{y^2}{y_\infty} + \frac{y^3}{3\left(y_\infty\right)^2} \tag{3.6.3}$$

$$v = \frac{du}{dy} = \frac{-2}{y_\infty^2}\left(y_\infty - y\right) \tag{3.6.4}$$

Similarly, differentiating equation (3.6.2) with respect to *y*, we get

$$t = \frac{dG}{dy} = \frac{-2}{y_\infty^2}\left(y_\infty - y\right) \tag{3.6.5}$$

Finally, to solve the problem of heat transfer coefficients of a continuous stretching surface we used Matlab® to program the Keller-box method. The complete program in this particular problem is given in appendix. Figure 3.2 below

shows the general flow diagram for the computations of the Keller-box method. The symbol are defined in Appendix.

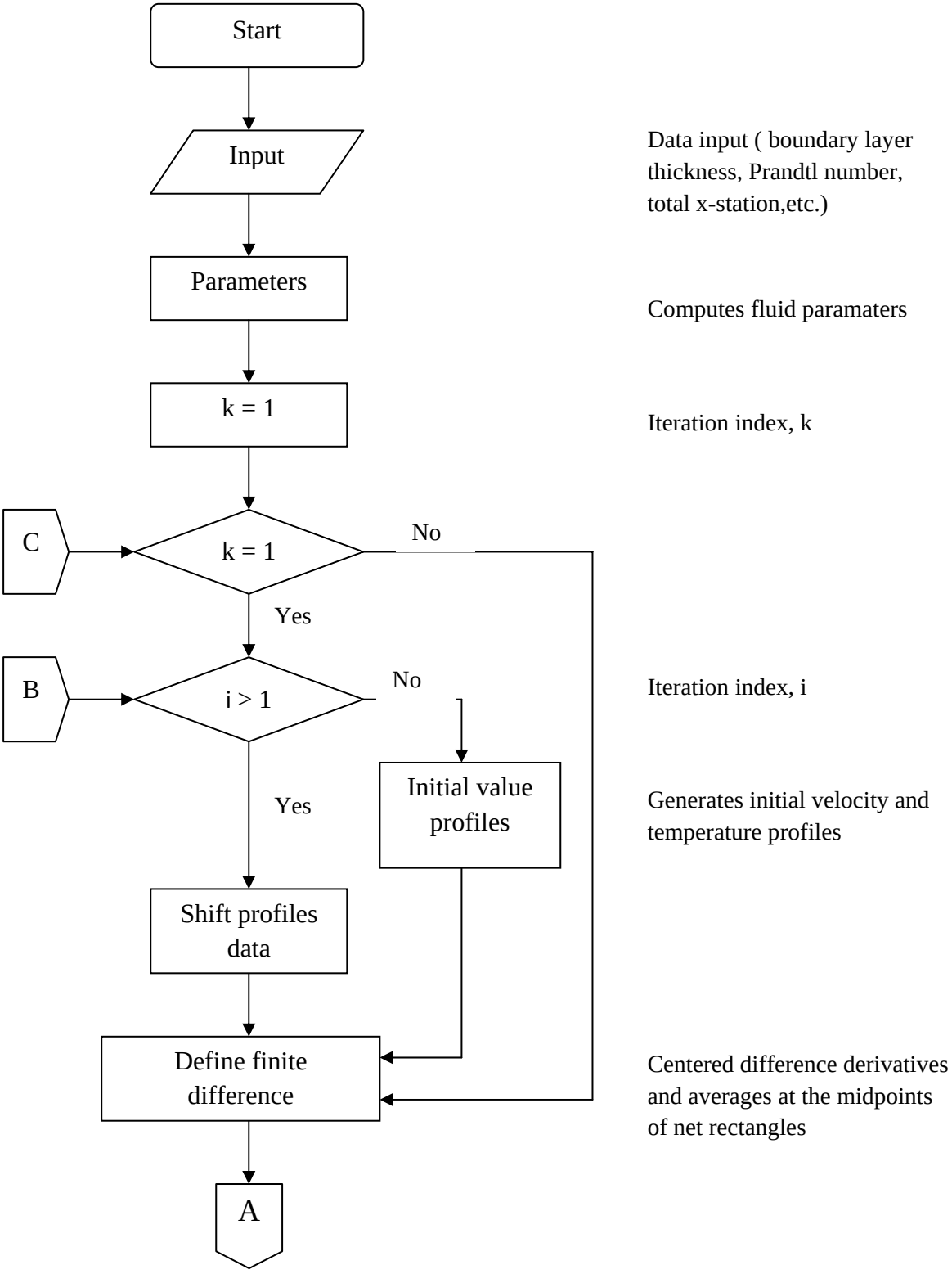

Figure 3.3 Flow diagrams for the Keller-box method

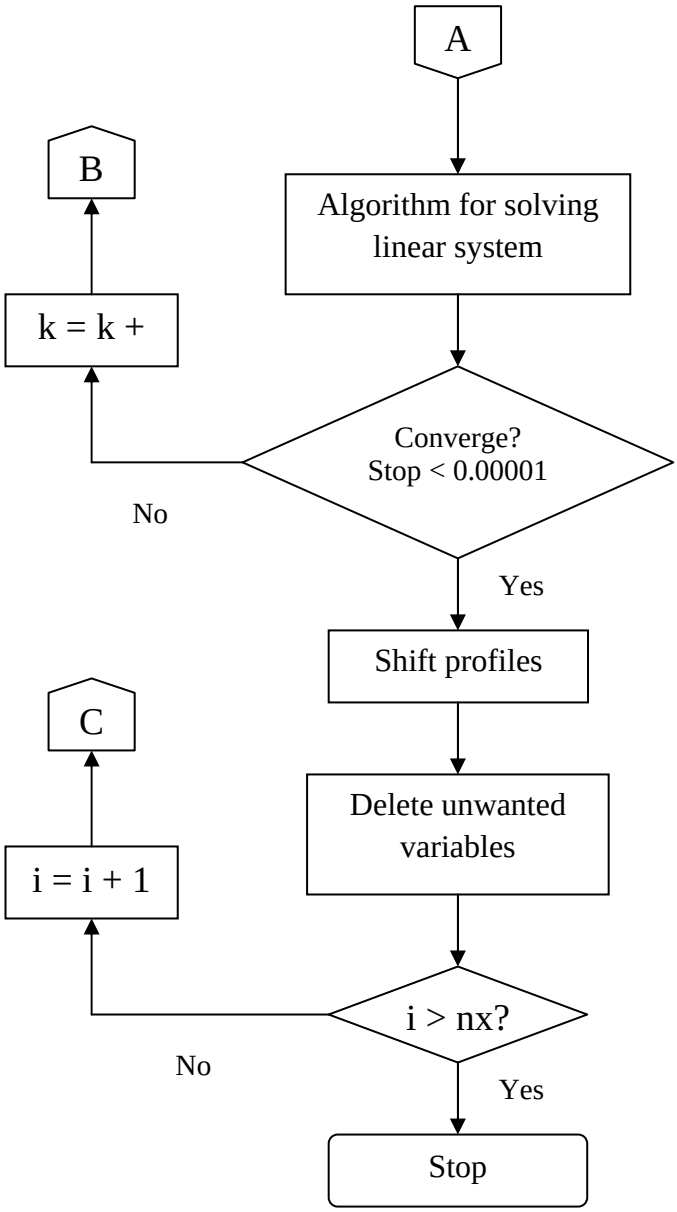

Figure 3.4 Flow diagrams for the Keller-box method (continued)

CHAPTER IV

HEAT TRANSFER COEFFICIENTS ON A CONTINOUOUS STRECTHING SURFACE

4.1 Introduction

In this chapter, the problem of heat transfer coefficients on a continuous stretching surface is considered and discussed. We will use the Keller-box method that has been described in Chapter 3 to solve this problem. Three cases of thermal boundary conditions, namely uniform surface temperature $(n = 0)$, variable surface temperature $(n \neq 0)$ and uniform heat flux $(n = (1-m)/2)$ are presented in the following three main section.

Section 4.2 will discuss the problem of heat transfer stretching surface with uniform surface temperature conditions and the result will be discussed in Section 4.2.1. The ordinary differential equations for problem with variable surface temperature are given in Section 4.3 and in Section 4.3.1 the result for this problem will be discussed. In the last section, Section 4.4 the problem for thermal boundary condition with uniform heat flux will be discussed and the results are presented in section 4.4.1.

4.2 Uniform Surface Temperature

Following Ali (1994), for uniform surface temperature case, we will consider the temperature exponent parameter, $n = 0$. According to equations (3.2.12) and (3.2.13), the ordinary differential equations for f and θ becomes

$$f''' + ff'' - \frac{2m}{m+1}\left(f'\right)^2 = 0 \tag{4.2.1}$$

$$\theta'' + \Pr f\theta' = 0 \tag{4.2.2}$$

subject to the boundary conditions

$$f'(0) = 1,\ f(0) = 0, \qquad \theta(0) = 1 \tag{4.2.3}$$

$$f'(\infty) = 0, \qquad \theta(\infty) = 0 \tag{4.2.4}$$

where primes denote differentiation with respect to η.

In practical applications, the physical quantity of principal interest is the local heat transfer coefficients, which can be expressed in terms of dimensionless parameters, Nusselt number *Nu* and Reynolds number *Re.* From Ali (1994) the heat transfer coefficients for uniform surface temperature case is given as

$$\frac{\mathrm{Nu}}{\sqrt{\mathrm{Re}}} = -\sqrt{\frac{m+1}{2}}\theta'(0) \tag{4.2.5 a}$$

In should mention that deriving equation (4.2.5 a) we had to use the definition of local heat transfer coefficient *h* and a local Nusselt number defined as

$$h = \frac{q_w}{T_w - T_\infty}, \quad Nu = \frac{hx}{k} \tag{4.2.5 b}$$

The heat transfer coefficients is important because in any practical situations, we have to know how strong a body is heated; the rate of heat transfer from the body

to the fluid; what kind of materials we have to use in order to avoid the body to be exposed to high temperatures, etc. All the practical devices that operate with the use of heat are designed based on theoretical or experimental heat transfer coefficients, such as nuclear devices, insulation of buildings.

4.2.1 Results and Discussion

Equation (4.2.1) and (4.2.2) subject to boundary conditions (4.2.3) and (4.2.4) were solved using the Keller-box. The solution procedure using this method has been discussed in Chapter III. All the results quoted here were obtained using uniform grid in η direction. We used the step size of $\Delta\eta = 0.05$. In all cases we choose $\eta = 10$. The initial profiles for this problem are given by equations (3.6.1) to (3.6.5).

Details results are for temperature profiles, $\theta(\eta)$ and heat transfer coefficient, $Nu/\sqrt{\mathrm{Re}}$ are obtained for the following values of velocity exponent parameter, $-0.41 \le m \le 3$ and $-3 \le m \le -1.1$ with Prandtl number, Pr = 0.72, 1.0, 3.0 and 10. In order to access the accuracy of the present method, we have compared the results for the heat transfer coefficient, $Nu/\sqrt{\mathrm{Re}}$ for $m = 0$ and $n = 0$ and temperature gradient $\theta'(0)$ for $m = 1$ and $n = 0$ with previously published result and found them into excellent agreement. The comparison is shown in Table 4.1 and Table 4.2. This favorable comparison lends confidence in the numerical results obtain in this paper.

Table 4.1: Heat transfer coefficient $\frac{Nu}{\sqrt{Re}}$ for $m = 0$ and $n = 0$.

Pr	Jacobi (1993)	Soundalgekar and Murty (1980)	Chen (1980)	Tsou et al (1967)	Ali (1994)	Present
0.7	0.3492	0.3508	0.3492	0.3492	0.3476	0.3493
1.0	0.4438	-	-	0.4438	0.4416	0.4438
10.0	1.6790	1.6808	-	1.6804	1.6713	1.6804

Table 4.2: Temperature gradient $\theta'(0)$ for $m = 1$ and $n = 0$.

Pr	Grubka and Bobba (1985)	Lakshmisha et al (1988)	Gupta (1977)	Ali (1994)	Present
0.7	-	0.45446	-	-0.45255	-0.4540
1.0	-0.5820	-	-0.5820	-0.59988	-0.5820
10.0	-2.3080	-	-	-2.29589	-2.3082
1.0	-	-	-0.1105	-0.10996	-0.1106

Figure 4.1 to 4.3 illustrate the dimensionless temperature profiles, $\theta(\eta)$ and heat transfer coefficient, $Nu/\sqrt{\mathrm{Re}}$ for various values of Prandtl numbers and velocity. Figure 4.1 shows that when $m = 3$ and $n = 0$ the thermal boundary layer thickness decreases for larger Prandtl numbers. From Figure 4.2, it is clear that increasing *m* from -0.25 to 3 changes the profile to be less flat near the edge of the boundary layer, while for *m* from -3 to -1.1 the profile change to be less steeper near the edge of the surface. These values of *m* mean that heat is transferred from continuous surface to the ambient (Ali, 1994).

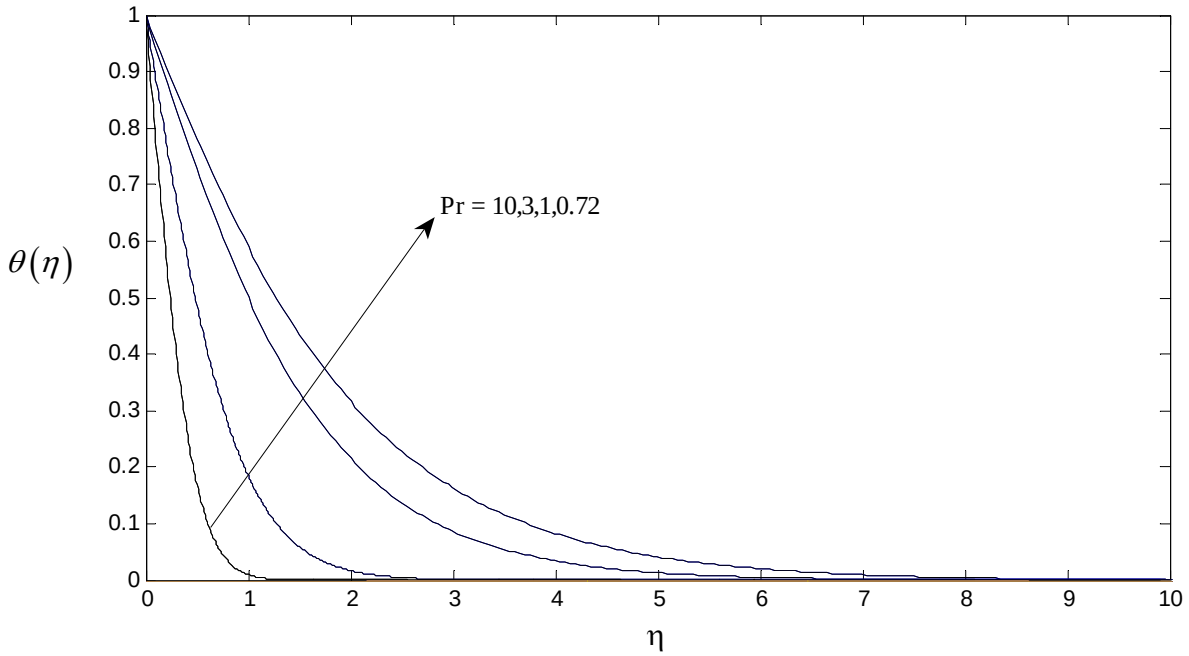

Figure 4.1: Dimensionless temperature profiles, $\theta(\eta)$ for various values of Prandtl numbers for $m = 3$ and $n = 0$.

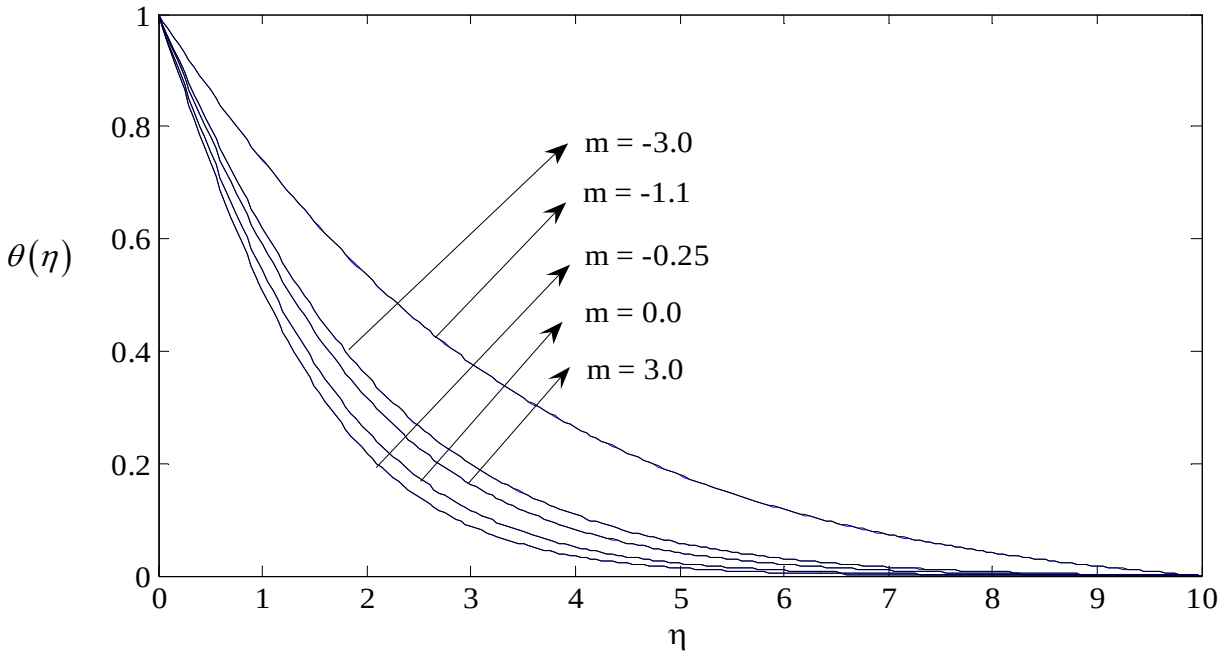

Figure 4.2: Dimensionless temperature profiles, $\theta(\eta)$ for various values of *m* for $n = 0$ and $\mathrm{Pr} = 0.72$.

Figure 4.3 presented the heat transfer coefficient in the dimensionless form of $Nu/\sqrt{\mathrm{Re}}$ as a function of *m* in the range of $-0.41 \le m \le 3$ for different Prandtl numbers. It shows that the increasing velocity exponent parameters, *m* and Prandtl number enhance the heat transfer coefficient, $Nu/\sqrt{\mathrm{Re}}$. Moreover, increasing Prandtl number increases the rate of heat transfer coefficient, $Nu/\sqrt{\mathrm{Re}}$.

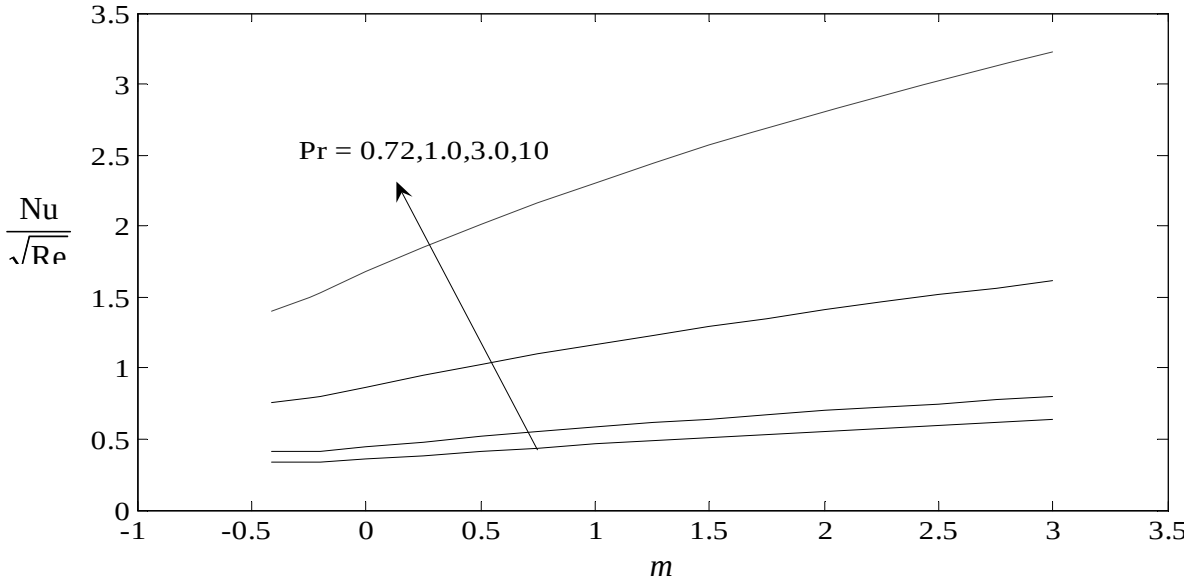

Figure 4.3: Variation of $\frac{Nu}{\sqrt{Re}}$ as a function of *m* at *n* = 0 and for different values of Prandtl number.

4.3 Variable Surface Temperature

In this section we will consider the variable surface temperature case $(n \neq 0)$. According to equations (3.2.12) and (3.2.13), the ordinary differential equations for f and θ becomes

$$f''' + ff'' - \frac{2m}{m+1}(f')^2 = 0 \tag{3.2.12}$$

$$\theta'' + \Pr\left[f\theta' - \frac{2n}{m+1} f'\theta \right] = 0 \tag{3.2.13}$$

subject to

$$f'(0) = 1,\ f(0) = 0, \qquad \theta(0) = 1 \tag{3.2.14}$$

$$f'(\infty) = 0, \qquad \theta(\infty) = 0 \tag{3.2.15}$$

where primes denote differentiation with respect to η.

In practical applications, the physical quantities of principal interest are the local heat transfer coefficients are same with the uniform surface temperature case.

4.3.1 Results and Discussion

Equation (3.2.12) and (3.2.13) subject to boundary conditions (3.2.14) and (3.2.15) were solved using the Keller-box. The solution procedure using this method has been discussed in Chapter III. All the results quoted here were obtained using uniform grid in η direction. We used the step size of $\Delta\eta = 0.05$. In all cases we choose $\eta = 10$. The initial profiles for this problem are given by equations (3.6.1) - (3.6.5).

Details results are for temperature profiles, $\theta(\eta)$ and heat transfer coefficient, $Nu/\sqrt{\mathrm{Re}}$ are obtained for the following values of velocity exponent parameter, $-0.41 \le m \le 3$ and $-3 \le m \le -1.1$ and temperature exponent parameter, $n \neq 0$ with Prandtl number, Pr = 0.72, 1.0, 3.0 and 10. The accuracy of this numerical method was validated by direct comparison with the numerical results reported earlier by Chen (1998), Grubka and Bobba (1985) and Ishak et al (2007) for $m = 1$. Table 4.3 present the temperature gradient, $\theta'(0)$, it can be seen from Table 4.3 that very good agreement between the results exists. This favorable comparison lends confidence in the numerical results obtained in this paper.

Table 4.3: Temperature gradient $\theta'(0)$ for $m = 1$.

	Grubka and Bobba (1985)			Ishak et al (2007)			Present		
n	Pr = 1	Pr = 3	Pr = 10	Pr = 1	Pr = 3	Pr = 10	Pr = 1	Pr = 3	Pr = 10
-2	1.0000	3.0000	10.0000	1.0000	3.0000	10.0000	0.9994	2.9999	9.9988
-1	0.0000	0.0000	0.0000	0.0000	0.0000	0.0000	-0.0001	0.0000	0.0000
0	-0.5820	-1.1652	-2.3080	-0.5820	-1.1652	-2.3080	-0.5820	-1.1653	-2.3081
1	-1.0000	-1.9237	-3.7207	-1.0000	-1.9237	-3.7207	-1.0000	-1.9237	-3.7208
2	-1.3333	-2.5097	-4.7969	-1.3333	-2.5097	-4.7969	-1.3333	-2.5097	-4.7970

Further, numerical results for temperature gradient, $\theta'(0)$ are presented in Table 4.4. The results presented in Table 4.4, show that $\theta'(0)$ is positive or negative then the direction of heat flow is to or from continuous stretching surface respectively. The dashed lines in this table at some Prandtl number indicate that unrealistic solutions (Grubka and Bobba, 1985) are obtained. For $0.5 \le m \le 3$ and $n < -2$, the temperature gradient, $\theta'(0)$ is positive, and the heat is transferred into the continuous surface from the ambient (Ali, 1994). However, for $-3 \le m \le -1.1$ the profiles switch their order with respect to *n*.

Table 4.4: Temperature gradient $\theta'(0)$ as a function of Prandtl numbers, temperature exponent and velocity exponent.

m	*n*	Pr = 0.72	Pr = 1.0	Pr = 3.0	Pr = 10.0
-0.41	0.00	-0.6288	-0.7672	-1.4023	-2.5802
-0.41	1.00	-1.6954	-2.0113	-3.4984	-6.3547
-0.41	2.00	-2.3340	-2.7555	-4.7614	-8.6437
-0.41	3.00	-2.8289	-3.3343	-5.7504	-10.4408
-0.25	-1.00	2.6328	4.9710	-	-
-0.25	0.00	-0.5449	-0.6737	-1.2834	-2.4435
-0.25	1.00	-1.3892	-1.6708	-3.0052	-5.5796
-0.25	2.00	-1.9376	-2.3123	-4.1021	-7.5736
-0.25	3.00	-2.3688	-2.8176	-4.9690	-9.1515
-0.20	-1.00	1.9120	3.1382	-	-
-0.20	0.00	-0.5328	-0.6602	-1.2663	-2.4240
-0.20	1.00	-1.3289	-1.6025	-2.9010	-5.4076
-0.20	2.00	-1.8555	-2.2193	-3.9570	-7.3281
-0.20	3.00	-2.2715	-2.7067	-4.7937	-8.8514
0.00	-1.00	0.8466	1.1892	3.7390	13.3456
0.00	0.00	-0.5038	-0.6276	-1.2246	-2.3764
0.00	1.00	-1.1547	-1.4035	-2.5891	-4.8818
0.00	2.00	-1.6113	-1.9401	-3.5124	-6.5638
0.00	3.00	-1.9776	-2.3699	-4.2515	-7.9103
0.50	-3.00	18.6243	-	-	-
0.50	-2.00	1.6657	2.6586	178.9910	-
0.50	-1.00	0.2054	0.2716	0.6283	1.3929
0.50	0.00	-0.4752	-0.5952	-1.1826	-2.3282
0.50	1.00	-0.9256	-1.1376	-2.1554	-4.1304
0.50	2.00	-1.2717	-1.5473	-2.8687	-5.4352
0.50	3.00	-1.5589	-1.8856	-3.4534	-6.5021
1.00	-3.00	2.2342	3.9915	-	-

1.00	-2.00	0.7167	0.9994	2.9999	9.9988
1.00	-1.00	-0.0011	-0.0001	0.0000	0.0000
1.00	0.00	-0.4636	-0.5820	-1.1653	-2.3081
1.00	1.00	-0.8088	-1.0000	-1.9237	-3.7208
1.00	2.00	-1.0886	-1.3333	-2.5097	-4.7970
1.00	3.00	-1.3270	-1.6153	-3.0000	-5.6935
1.50	-3.00	1.1227	1.6526	7.5935	-
1.50	-2.00	0.3732	0.5027	1.2569	3.0542
1.50	-1.00	-0.1057	-0.1348	-0.2889	-0.6014
1.50	0.00	-0.4573	-0.5748	-1.1557	-2.2969
1.50	1.00	-0.7373	-0.9151	-1.7779	-3.4603
1.50	2.00	-0.9725	-1.1965	-2.2769	-4.3799
1.50	3.00	-1.1769	-1.4393	-2.7016	-5.1583
2.00	-3.00	0.6862	0.9558	2.8438	9.3630
2.00	-2.00	0.1910	0.2540	0.5943	1.3385
2.00	-1.00	-0.1694	-0.2159	-0.4576	-0.9446
2.00	0.00	-0.4533	-0.5702	-1.1496	-2.2898
2.00	1.00	-0.6889	-0.8573	-1.6774	-3.2794
2.00	2.00	-0.8918	-1.1010	-2.1126	-4.0838
2.00	3.00	-1.0711	-1.3146	-2.4884	-4.7741
2.50	-3.00	0.4467	0.6070	1.5786	4.0562
2.50	-2.00	0.0770	0.1024	0.2319	0.5054
2.50	-1.00	-0.2123	-0.2703	-0.5688	-1.1681
2.50	0.00	-0.4505	-0.5670	-1.1454	-2.2849
2.50	1.00	-0.6540	-0.8153	-1.6037	-3.1461
2.50	2.00	-0.8324	-1.0304	-1.9899	-3.8618
2.50	3.00	-0.9922	-1.2213	-2.3276	-4.4833
3.00	-3.00	0.2938	0.3939	0.9603	2.2664
3.00	-2.00	-0.0015	-0.0002	0.0000	0.0000
3.00	-1.00	-0.2432	-0.3093	-0.6479	-1.3259
3.00	0.00	-0.4485	-0.5647	-1.1423	-2.2813
3.00	1.00	-0.6275	-0.7835	-1.5474	-3.0438
3.00	2.00	-0.7868	-0.9759	-1.8947	-3.6889
3.00	3.00	-0.9309	-1.1486	-2.2015	-4.2548
3.50	-2.00	-0.0589	-0.0745	-0.1623	-0.3433
4.50	-3.00	0.0469	0.0632	0.1426	0.3097
5.00	-3.00	-0.0016	-0.0002	0.0000	0.0000
-3.00	-3.00	-1.2329	-1.5157	-2.8882	-5.5745
-3.00	-2.00	-1.0022	-1.2404	-2.4024	-4.6810
-3.00	-1.00	-0.7353	-0.9189	-1.8249	-3.6111
-3.00	0.00	-0.4140	-0.5246	-1.0877	-2.2164
-3.00	1.00	-0.0026	-0.0004	0.0000	0.0000
-3.00	2.00	0.5794	0.8061	2.3397	7.4432
-3.00	3.00	1.5674	2.5042	-	-
-2.00	-3.00	-1.7543	-2.1388	-4.0028	-7.6507
-2.00	-2.00	-1.4005	-1.7195	-3.2699	-6.3082

-2.00	-1.00	-0.9703	-1.2057	-2.3611	-4.6358
-2.00	0.00	-0.3966	-0.5041	-1.0589	-2.1815
-2.00	0.50	-0.0035	-0.0007	0.0000	0.0000
-2.00	1.00	0.5363	0.7468	2.1521	6.7742
-2.00	2.00	3.2501	7.8899	-	-
-1.50	-3.00	-2.5093	-3.0409	-5.6223	-10.6746
-1.50	-2.00	-1.9910	-2.4282	-4.5539	-8.7199
-1.50	-1.00	-1.3391	-1.6540	-3.1953	-6.2280
-1.50	0.00	-0.3697	-0.4717	-1.0119	-2.1232
-1.50	0.30	0.0792	0.1114	0.2707	0.6337
-1.50	1.00	2.4167	4.6876	-6.5541	-1.3821
-1.15	-3.00	-4.6355	-5.5889	-10.2370	-19.3241
-1.15	-2.00	-3.6719	-4.4505	-8.2486	-15.6877
-1.15	-1.00	-2.4330	-2.9831	-5.6776	-10.9786
-1.15	0.00	-0.3018	-0.3865	-0.8767	-1.9445
-1.10	-3.00	-5.6861	-6.8493	-12.5345	-23.6380
-1.10	-2.00	-4.5044	-5.4537	-10.0931	-19.1739
-1.10	-1.00	-2.9808	-3.6498	-6.9299	-13.3807
-1.10	0.00	-0.2761	-0.3525	-0.8164	-1.8587

Figure 4.4 to 4.7 illustrate the dimensionless temperature profiles, $\theta(\eta)$ and heat transfer coefficient, $Nu/\sqrt{\mathrm{Re}}$ for various values of Prandtl numbers, velocity exponent parameter *m* and temperature exponent parameter *n*. Figure 4.4 shows that when $\mathrm{Pr} = 0.72$ and $m = 3$ it is clear that increasing value of *n* change the profile to be more flat near the edge of the boundary layer. Furthermore, when *n* is increase in the range $n > -2$ the boundary layer profile change to be steeper near the edge of the surface and this means that the heat is transferred from the continuous stretching surface to the fluid medium (Ali, 1994). Figure 4.5 presented the dimensionless temperature profiles θ for $m = -0.25$ and $n = -1$. In this figure, for Prandtl number 0.72 and 1.0 heat is transferred to the surface however for Prandtl number 3.0 and 10.0 heat is transferred from the surface to the ambient.

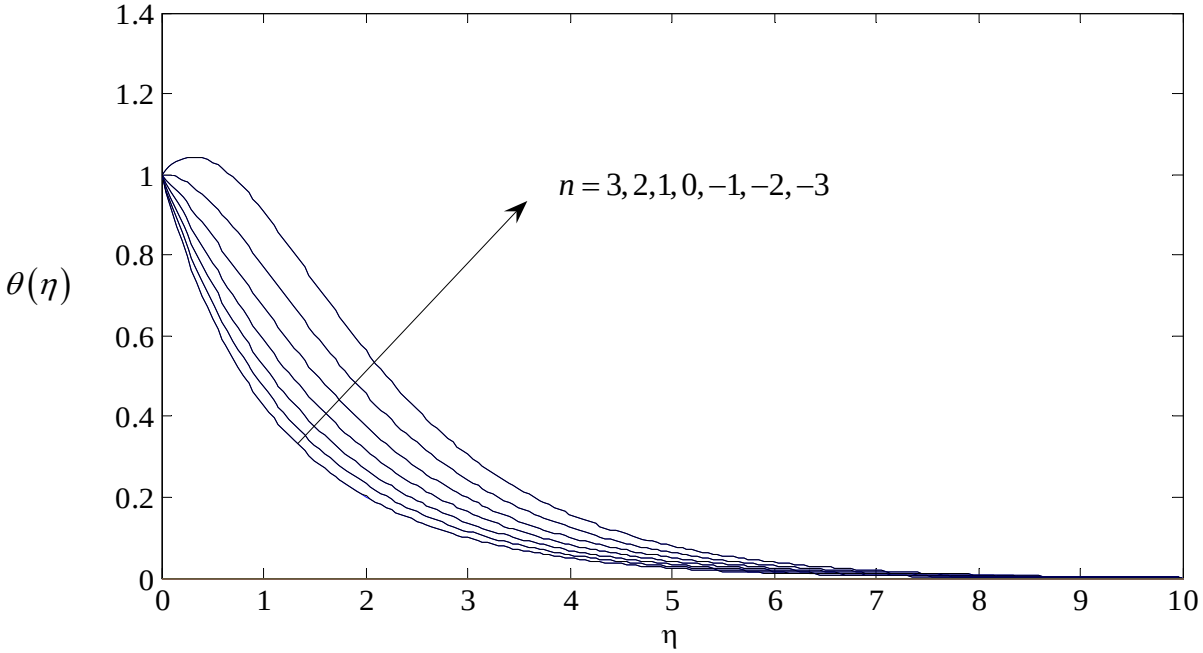

Figure 4.4: Dimensionless temperature profiles, $\theta(\eta)$ for various values of n for $m = 3$ and $\Pr = 0.72$.

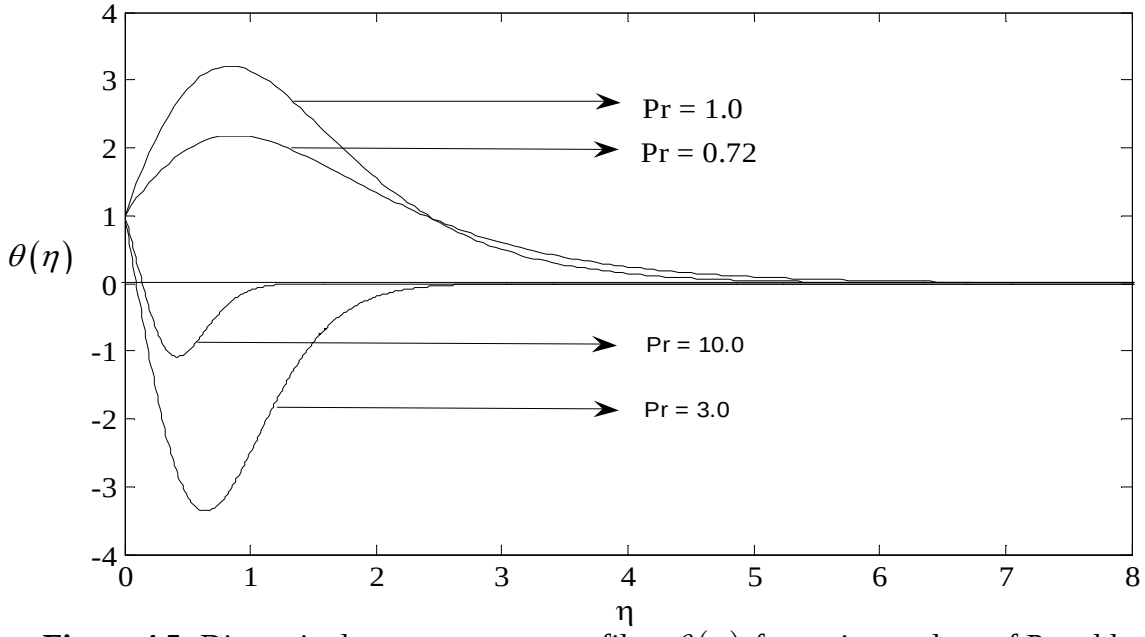

Figure 4.5: Dimensionless temperature profiles, $\theta(\eta)$ for various values of Prandtl numbers for $m = -0.25$ and $n = -1$.

The variation of heat transfer coefficient, $Nu/\sqrt{\mathrm{Re}}$ for $n = -1$ is presented in Figure 4.6. It is clear that for $-0.25 \le m \le 1$ heat is transferred from the fluid to the

surface for all values of Prandtl numbers and at $m = 1$ it is adiabatic surface and there is no heat exchange between the surface and the fluid medium. However for $m > 1$ heat is transferred from the surface to the ambient for all values of Prandtl numbers. We notice that in Figure 4.7 when $n = 2$, heat is transferred from the continuous stretching surface to the fluid medium. We also see from Figure 4.6 and 4.7 that the increasing of *n*, *m* and Prandtl numbers enhances the heat transfer coefficient, $Nu/\sqrt{\mathrm{Re}}$.

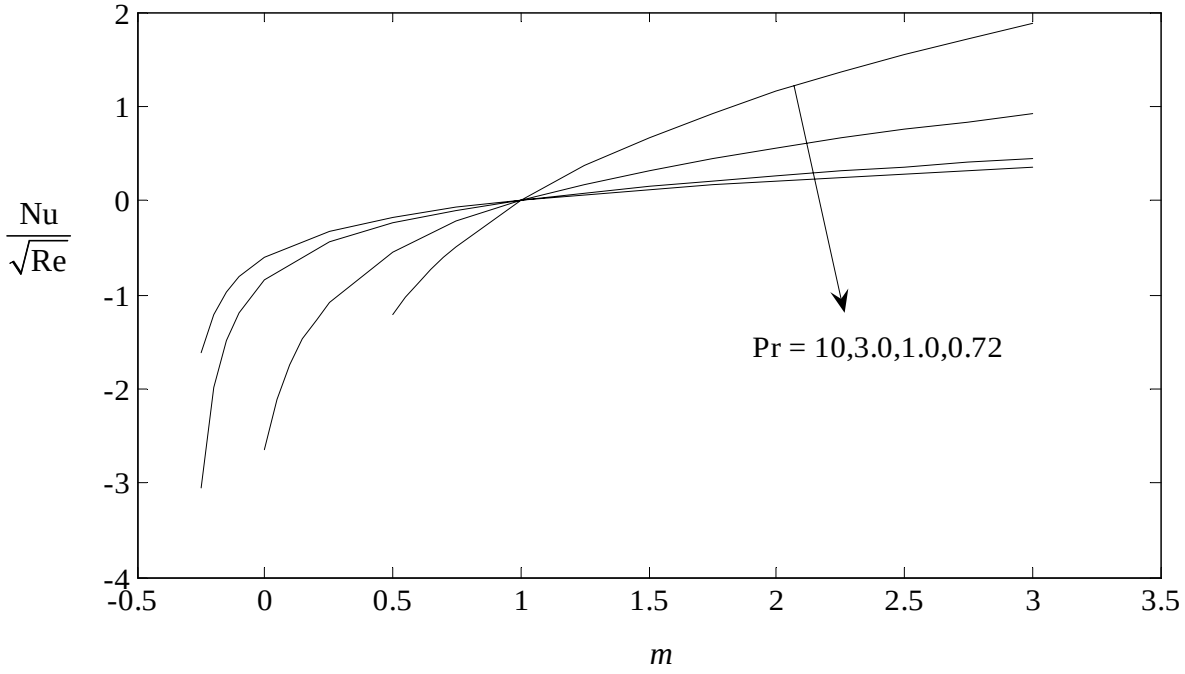

Figure 4.6: Variation of $\frac{Nu}{\sqrt{Re}}$ as a function of *m* at *n* = -1 and for different values of Prandtl number.

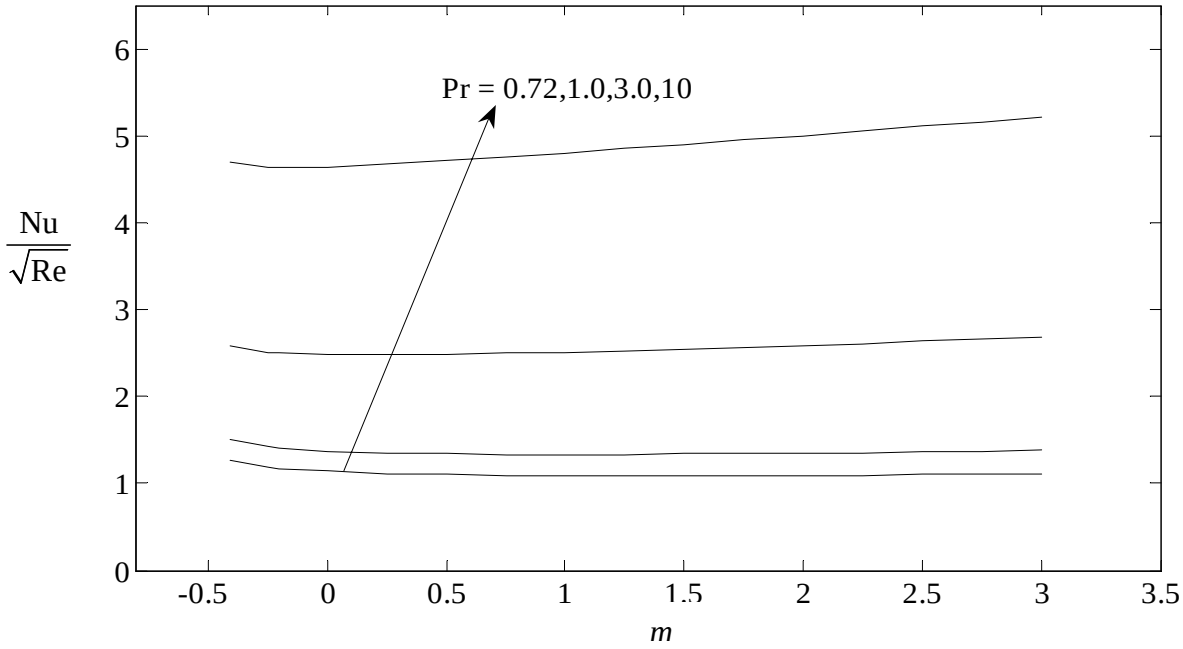

Figure 4.7: Variation of $\frac{Nu}{\sqrt{Re}}$ as a function of *m* at *n* = 2 and for different values of Prandtl number.

4.4 Uniform Heat Flux

In this case, we will consider the temperature exponent parameter, $n=(1-m)/2$. According to equations (3.2.12) and (3.2.13), the ordinary differential equations for f and θ becomes

$$f''' + ff'' - \frac{2m}{m+1}(f')^2 = 0 \tag{4.4.1}$$

$$\theta'' + \Pr\left[f\theta' - \left(\frac{1-m}{m+1}\right) f'\theta \right] = 0 \tag{4.4.2}$$

subject to the boundary conditions

$$f'(0) = 1,\ f(0) = 0, \qquad \theta'(0) = -1 \tag{4.4.3}$$

$$f'(\infty)=0, \qquad \theta(\infty)=0 \tag{4.4.4}$$

where primes denote differentiation with respect to η

In practical applications, the physical quantities of principal interest are the local heat transfer coefficients, which can be expressed in terms of dimensionless parameters, Nusselt number *Nu* and Reynolds number *Re.* From Ali (1994) the heat transfer coefficients for uniform surface temperature case is

$$\frac{\mathrm{Nu}}{\sqrt{\mathrm{Re}}}=\frac{\sqrt{\frac{m+1}{2}}}{\theta(0)} \tag{4.4.5}$$

4.4.1 Results and Discussion

Equation (4.4.1) and (4.4.2) subject to boundary conditions (4.4.3) and (4.4.4) were solved using the Keller-box. The solution procedure using this method has been discussed in Chapter III. The element of matrix ***A*** in the correlation (3.5.1) have some differences, where the equations (3.5.2a) and (3.5.5a) becomes

$$[A_1]=\begin{bmatrix} 0 & 0 & 1 & 0 & 0 \\ d_1 & 0 & 0 & d_1 & 0 \\ 0 & -1_1 & 0 & 0 & d_1 \\ (a_2)_1 & 0 & (a_3)_1 & (a_1)_1 & 0 \\ 0 & (b_2)_1 & (b_3)_1 & 0 & (b_1)_1 \end{bmatrix}, \text{ and } [\delta_1]=\begin{bmatrix} \delta v_0 \\ \delta t_0 \\ \delta f_1 \\ \delta v_1 \\ \delta t_1 \end{bmatrix} \tag{4.4.6 a,b}$$

The corresponding boundary conditions are

$$f_0^n=0, \quad u_0^n=1, \quad t_0^n=-1, \quad u_j^n=0, \quad v_j^n=0, \quad G_j^n=0 \tag{4.4.7}$$

and

$$\delta f_0 = 0, \quad \delta u_0 = 0, \quad \delta t_0 = 0, \quad \delta u_J = 0, \quad \delta v_J = 0, \quad \delta G_J = 0 \tag{4.4.8}$$

All the results quoted here were obtained using uniform grid in η direction. We used the step size of $\Delta\eta = 0.05$. In all cases we choose $\eta = 10$. The initial of the velocity profile are the same as the equations (3.6.1), (3.6.2) and (3.6.3) while the initial values of temperature profile is adopted from the uniform heat flux problem that is given by Lienhard (1981) as follows

$$G = \theta = \frac{y_\infty}{2}\left(1 - \frac{y}{y_\infty}\right)^2 \tag{4.4.9}$$

and initial values for temperature gradient profile is

$$t = \frac{\left(y_\infty - y\right)}{y_\infty} \tag{4.4.10}$$

Details results are for temperature profiles, $\theta(\eta)$ and heat transfer coefficient, $Nu/\sqrt{\mathrm{Re}}$ are obtained for the following values of velocity exponent parameter, $-0.41 \le m \le 3$, $-3 \le m \le -1.1$ and Prandtl number, Pr = 0.72, 1.0, 3.0 and 10. Figure 4.8 to 4.10 illustrate the dimensionless temperature profiles, $\theta(\eta)$ and heat transfer coefficient, $Nu/\sqrt{\mathrm{Re}}$ for various values of Prandtl numbers, velocity exponent parameter, *m* and temperature exponent parameter, *n*. From figure 4.8, the thermal boundary layer is increasing with increasing *m* and this means that more heat is dissipated to the fluid medium. However, the effect of decreasing the boundary layer thickness with increasing Prandtl number is shown in Figure 4.9 for $m = -0.41$.

The heat transfer coefficient, $Nu/\sqrt{\mathrm{Re}}$ is presented in Figure 4.10. This figure indicates that increasing Prandtl number enhances the heat transfer coefficient, $Nu/\sqrt{\mathrm{Re}}$. However, compared to the two cases previously uniform surface temperature and variable surface temperature, we found that in this case the heat transfer coefficient, $Nu/\sqrt{\mathrm{Re}}$ decreases with increasing *m*.

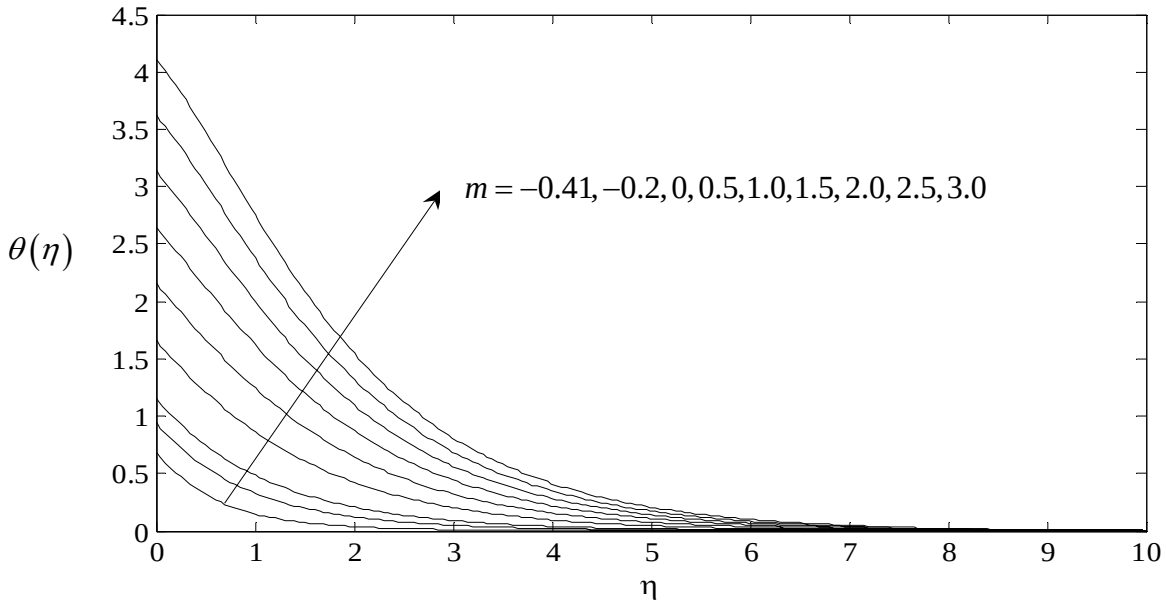

Figure 4.8: Dimensionless temperature profiles, $\theta(\eta)$ for various values of m for and $\Pr = 0.72$.

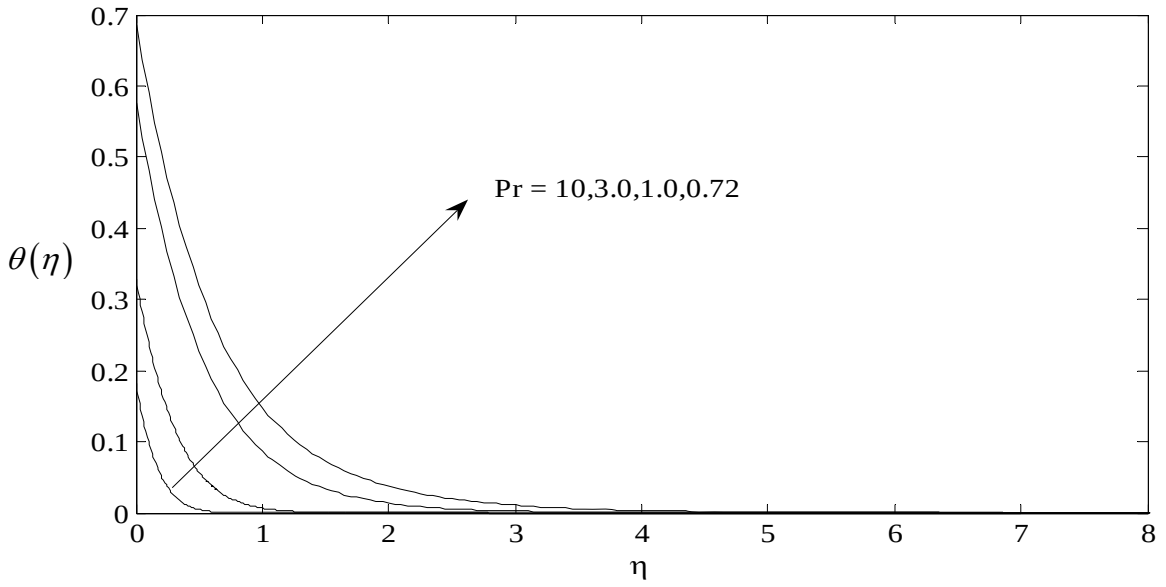

Figure 4.9: Dimensionless temperature profiles, $\theta(\eta)$ for various values of Prandtl number and $m = -0.41$.

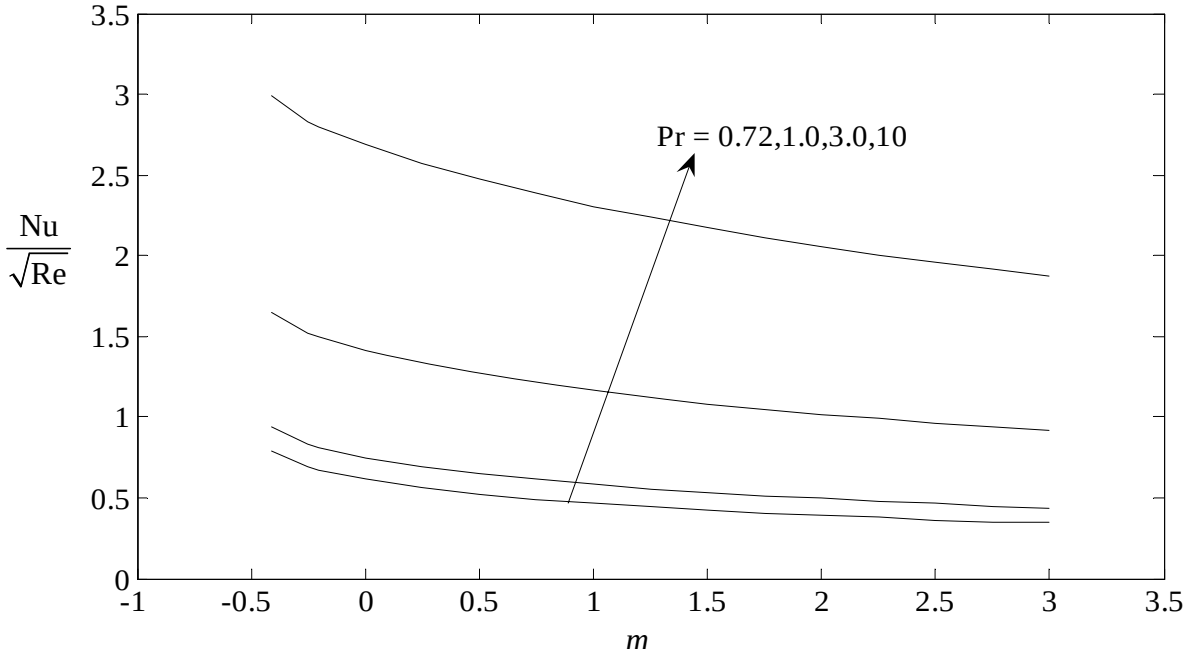

Figure 4.10: Variation of $\frac{Nu}{\sqrt{Re}}$ as a function of *m* at different values of Prandtl number.

CHAPTER V

g-JITTER FREE CONVECTION ADJACENT TO A VERTICAL STRECHING SHEET

5.1 Introduction

In this chapter, the problem of g-jitter free convection adjacent to vertical stretching sheet is considered and discussed. We will also use the Keller-box method that has been described in Chapter 3 to solve this problem. Section 5.2 will discuss the basic equations of the problem. Finally, in Section 5.3 the result for this problem will be discussed.

5.2 Basic Equations

Consider the g-jitter flow of a viscous and incompressible fluid over a vertical sheet as shown in Figure 1. Two equal and opposite forces are impulsively applied along the *x*-axis so that the wall is stretched, keeping the origin fixed in a viscous and incompressible fluid of ambient temperature T_∞. The temperature of the plate is assumed to be suddenly increased or decreased to the value T_∞. The stationary coordinate system has its origin located at the center of the sheet with the positive *x*-axis extending along the sheet in the upward direction, while the *y*-axis is measured normal to the surface of the sheet and is positive in the direction from the sheet to the fluid. The continuous stretching surface is assumed to have the velocity and temperature of the form $u_w(x) = c\,x$ and $T_w(x) = T_\infty + a\,x$, where a and c are constants and $c > 0$. Both the cases of heating $(T_w > T_\infty)$ or cooling $(T_w < T_\infty)$ of the

sheet will be considered, which correspond to $a > 0$ or $a < 0$, respectively.

Under these assumptions along with the Boussinesq and boundary layer approximations, the basic equations are

$$\frac{\partial u}{\partial x}+\frac{\partial v}{\partial y}=0 \tag{5.2.1}$$

$$\frac{\partial u}{\partial t}+u\frac{\partial u}{\partial x}+v\frac{\partial u}{\partial y}=\upsilon\frac{\partial^2 u}{\partial y^2}+g^*(t)\,\beta\,(T-T_\infty) \tag{5.2.2}$$

$$\frac{\partial T}{\partial t}+u\frac{\partial T}{\partial x}+v\frac{\partial T}{\partial y}=\alpha\,\frac{\partial^2 T}{\partial y^2} \tag{5.2.3}$$

subject to the initial and boundary conditions

$$\begin{aligned} &t<0: u=v=0,\ T=T_\infty \ \text{ any } \ x, y\\ &t>0: u_w(x)=\ c\,x,\ v=0,\ T_w(x)=T_\infty+a\,x \ \text{ on } \ y=0\\ &u\to 0,\ T\to T_\infty \ \text{ as } \ y\to\infty \end{aligned} \tag{5.2.4}$$

where u and v are the velocity components along x- and y- axes, T is the fluid temperature, α, β and υ are the thermal diffusivity, the thermal expansion coefficient and kinematic viscosity, respectively. We now define the following non-dimensional variables

$$\begin{aligned} &\tau=\omega t,\ \eta=\ (\frac{c}{\upsilon})^{\frac{1}{2}}y,\ \psi=\ (c\upsilon)^{\frac{1}{2}}x\,f(\tau,\eta)\\ &\theta(\tau,\eta)=\frac{(T-T_\infty)}{(T_w-T_\infty)},\ g(\tau)=\frac{g^*(t)}{g_0} \end{aligned} \tag{5.2.5}$$

where ψ is the stream function which is defined as $u=\dfrac{\partial\psi}{\partial y}$ and $v=-\dfrac{\partial\psi}{\partial x}$. With the use of (5.2.5), equations (5.2.2) and (5.2.3) become

$$\frac{\partial^3 f}{\partial \eta^3} + f\frac{\partial^2 f}{\partial \eta^2} - \left(\frac{\partial f}{\partial \eta}\right)^2 + \lambda\left[1+\varepsilon\cos(\pi\tau)\right]\theta = \Omega\frac{\partial^2 f}{\partial \tau\,\partial \eta} \tag{5.2.6}$$

$$\frac{1}{Pr}\frac{\partial^2 \theta}{\partial \eta^2} + f\frac{\partial \theta}{\partial \eta} - \frac{\partial f}{\partial \eta}\theta = \Omega\frac{\partial \theta}{\partial \tau} \tag{5.2.7}$$

and the boundary conditions (5.2.4) become

$$\begin{aligned} &f = 0,\ \frac{\partial f}{\partial \eta} = 1,\ \theta = 1 \ \text{ on } \ \eta = 0 \\ &\frac{\partial f}{\partial \eta} \to 0,\ \theta \to 0 \ \text{ as } \ \eta \to \infty \end{aligned} \tag{5.2.8}$$

where $\Omega = \dfrac{\omega}{c}$ is the non-dimensional frequency and λ is the mixed convection parameter , which is defined as

$$\lambda = \frac{g_0\,\beta\,[T_w(x) - T_\infty]\dfrac{x^3}{\upsilon^2}}{[u_w(x)\dfrac{x}{\upsilon}]^2} = \frac{Gr_x}{Re_x^2} \tag{5.2.9}$$

with $Gr = g_0\,\beta[T_w(x) - T_\infty]\dfrac{x^3}{\upsilon^2}$ being the local Grashof number and $Re = u_w(x)\dfrac{x}{\upsilon}$ is the local Reynolds number, respectively. We notice that $\lambda > 0$ corresponds to an aiding flow and $\lambda < 0$ corresponds to an opposing flow, respectively.

The physical quantities of interest include the reduced velocity $f'(\eta)$ and the non-dimensional temperature profiles as well as the skin friction coefficient, C_f , and the local Nusselt number, Nu , which are defined as

$$C_f = \frac{\tau_w(x)}{\left(\dfrac{\rho u_w^2}{2}\right)}, \quad Nu_x = \frac{q_w(x)\,x}{k\,(T_w - T_\infty)} \tag{5.2.10}$$

where the $\tau_w(x)$ and $q_w(x)$ are given by

$$\tau_w = \mu(\frac{\partial u}{\partial y})_{y=0}, \quad q_w(x) = -k(\frac{\partial T}{\partial y})_{y=0} \tag{5.2.11}$$

k being the thermal conductibility. Using variables (5.2.5), we get

$$C_f \, Re_x^{\frac{1}{2}} = 2\,\frac{\partial^2 f}{\partial \eta^2}(\tau,0) \quad \frac{Nu_x}{Re_x^{\frac{1}{2}}} = -\frac{\partial \theta}{\partial \eta}(\tau,0) \tag{5.2.12}$$

We notice that when g-jitter is absent, e.g., when the parameter ε of the amplitude of the modulation is zero ($\varepsilon = 0$), equations (5.2.6) and (5.2.7) reduce to

$$f'''+ f\, f''- f'^2+\lambda\theta = 0 \tag{5.2.13}$$

$$\theta''+\Pr(f\,\theta'- f'\theta) = 0 \tag{5.2.14}$$

and the boundary conditions (4.2.8) become

$$\begin{aligned} &f(0) = 0, \;\; f'(0) = 1, \;\; \theta(0) = 1 \\ &f'(\infty) = 0, \;\; \theta(\infty) = 0 \end{aligned} \tag{5.2.15}$$

where primes denote differentiation with respect to η. The skin friction coefficient and the Nusselt number given by equations (5.2.12) are now given by

$$C_f Re_x^{\frac{1}{2}} = 2\, f''(0), \;\; \frac{Nu_x}{Re_x^{\frac{1}{2}}} = -\theta'(0) \tag{5.2.16}$$

5.3 Results and Discussion

The two sets of transformed differential equations (5.2.6) to (5.2.8) and

(5.2.13) to (5.2.15) have been solved numerically using the Keller-box method described in the book by Cebeci and Bradshaw (1984). We first solved equations (5.2.13) to (5.2.15) for different values of the Prandtl number Pr , the mixed convection parameter $\lambda > 0$ (assisting flow) and $\lambda < 0$ (opposing flow), respectively. To assess the accuracy of the present numerical method, comparison of the wall heat flux, $-\theta'(0)$ is made with those of Grubka and Bobba (1985). It can be seen from Table 5.1 that for some values of Pr when the buoyancy effect is neglected (λ=0), the results are in very good agreement, thus ensuring that the present method is accurate.

Table 5.1: Comparison of heat transfer rate $\theta'(0)$ for $\lambda = 0$ and various values of Pr.

	0.01	0.72	1.0	3.0	10.0	100.0
Present Results	-0.0199	-0.8086	-1.0000	-1.9238	-3.7225	-12.3953
Grubka and Bobba [26]	-0.0197	-0.8086	-1.0000	-1.9237	-3.7207	-12.2940

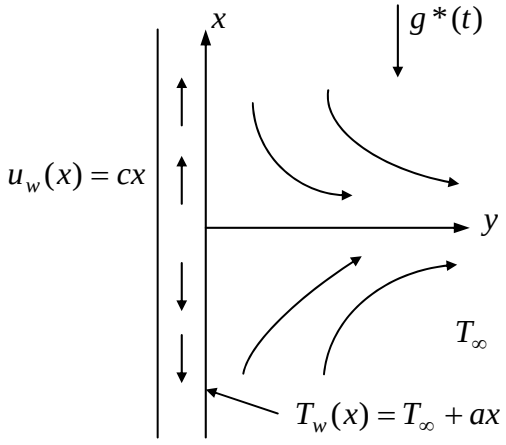

Figure 5.1: Physical model and coordinate system.

Further, we have found that equations (5.2.13) to (5.2.15) have solutions for any values $\lambda > 0$ (assisting flow), but for $\lambda < 0$ (opposing flow), these equations have solutions only for values of $\lambda_c(Pr) < \lambda (< 0)$. $\lambda_c(Pr)$ is a critical value of λ for which a solution of equations (14) to (16) exists while for values of $\lambda < \lambda_c(Pr) < 0$, a solution of these equations does not exist. Table 5.2 contains values of $\lambda_c(Pr)$, $f''(0)$ and $-\theta'(0)$ for some values of Pr. Figures 5.2 and 5.3 illustrate the variation of the reduced skin friction, $f''(0)$, and heat transfer parameter, $-\theta'(0)$,

with λ for some values of *Pr*. It can be seen from this table and figures that $-\theta'(0)$ increases continuously with λ positive or negative, while the assisting flow ($\lambda > 0$), produces an increase in $f''(0)$ and an opposing flow ($\lambda < 0$) produces a decrease in $f''(0)$, respectively. We notice that increasing the value of *Pr*, will increase the values of $-\theta'(0)$ that is increasing *Pr* enhances the heat transfer at the sheet. Thus, fluids having a smaller Prandtl number are more sensitive to the buoyancy force than fluids with a larger Prandtl number. These results are in agreement with those reported by Chen (1998), see Figures 3b and 4b in his paper.

Table 5.2: Values of $f''(0)$ and $\theta'(0)$ for critical values of λ_c (<0) and different values of *Pr*.

	λ_c	$f''(0)$	$-\theta'(0)$
0.70	-0.26653	-1.20032	0.69854
0.72	-0.27355	-1.20268	0.71280
1.00	-0.39356	-1.24525	0.89693
3.00	-2.01309	-1.75017	1.72057
7.00	-6.08544	-2.61278	2.67616
10.00	-9.23648	-3.11007	3.21465
50.00	-52.35663	-6.88706	7.28834
100.00	-103.75937	-10.03744	10.10021

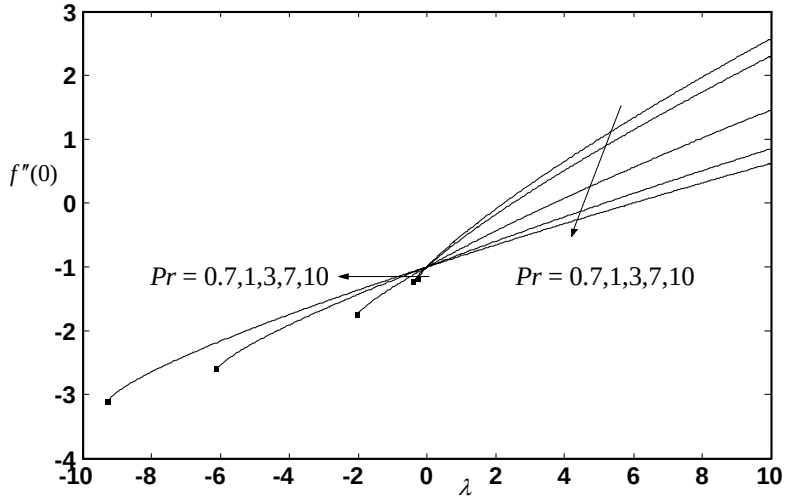

Figure 5.2: Variations of the skin friction with λ for different values of Pr.

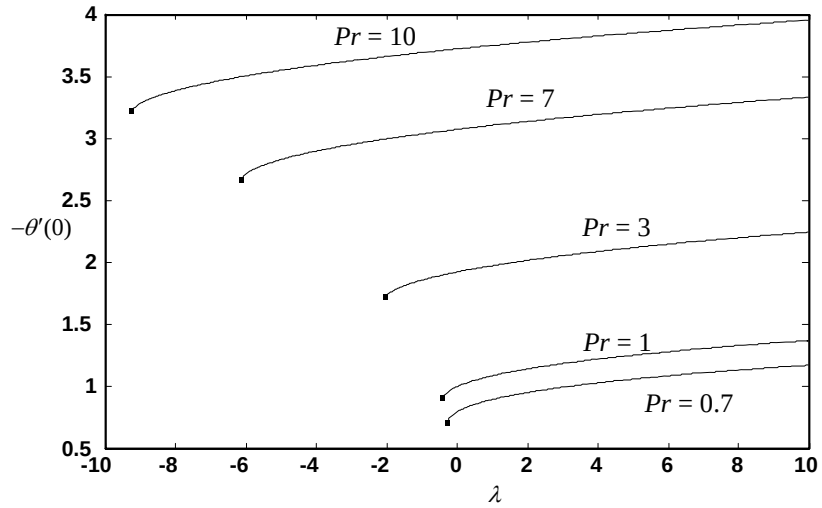

Figure 5.3: Variations of the heat flux with λ for different values of Pr.

Further, we have solved numerically equations (5.2.6) to (5.2.8) for several values of the governing parameters ε, Ω and λ_c with Pr = 0.72 (air) and 6.8 (water), respectively. In all the results we vary ε from 0 to 1 since values of ε above 1 is equivalent to having the perceived gravity reverse its direction over part of the g-jitter cycle. The computations were always started with the appropriate steady solution to the ε = 0 case and convergence to a steady periodic state was demanded to have taken place when

$$\max\left|\theta'(\tau,0)-\theta'(\tau-2,0)\right|<10^{-6} \tag{5.3.1}$$

over a whole period. The results are summarized in Tables 5.3 and 5.4 and in Figures 5.4 to 5.11. Tables 5.2 and 5.3 contain the values of the mean heat transfer rate $\Theta'(0)$ and the mean skin friction $F''(0)$ over one period using trapezoidal rule to obtain their respective means. We can notice a very clear difference between these tables due to the different values of Pr and λ_c. However, it can be seen that the overall effect of even very large g-jitter amplitudes Ω on the rate of heat transfer and the skin friction is fairly small. Figures 5.4 to 5.7 show the variation of the skin friction quantity, $-f''(\tau,0)$, and surface heat transfer, $-\theta'(\tau,0)$, for Pr = 0.72 and 6.8, Ω = 0.2, 1 and 5, λ_c = -0.13 and -2.13 (opposing flow) and some values of ε. All Figures 5.4 to 5.7 show that the effect of increasing ε is to give an almost proportional increase or decrease in skin friction and heat transfer. The upper and

lower peaks occur near $\tau = 0.5$ and 1.5 for heat transfer, as can be seen from Figures 5.4 and 5.6 but the peaks in the response occur after these values. The corresponding curves for heat transfer show different trends as can be seen from Figures 5.5 and 5.7. However, the main differences between Figures 5.4 to 5.7 lie in the range of values that $-f''(\tau,0)$ and $-\theta'(\tau,0)$ take, which is clearly related to the values of *Pr*. When *Pr* increases, the thermal conductivity decreases in importance relative to the viscosity, and advection occurs more easily than conduction. Therefore, the thermal boundary layer decreases in thickness as *Pr* increases, and this is the cause in the overall increase in the value of the surface rate of heat transfer. However it depends also on the buoyancy parameter λ. Thus the heat transfer increases when both $\lambda(<0)$ and Pr increase as shown in Figures 5.5 and 5.7. Finally, the influence of the mixed convection parameter λ and Ω on the time-periodic flow is shown in Figures 5.8 to 5.11. Here we have chosen ε = 0.5, and the same values of *Pr* and Ω as above, but a wider range of values of λ than is used in the previous figures. It can be seen from Figures 5.8 to 5.11 that the changes in the peak response in both $-f''(\tau,0)$ and $-\theta'(\tau,0)$ are seen to be more substantial for an opposing flow $(\lambda<0)$ than for an assisting flow $(\lambda>0)$, respectively. But, as *Pr* and Ω increase, the peak response for the rate of heat transfer progressively disappears. Indeed, the rate of heat transfer is almost constant when Ω > 5, as can be seen from Figures 5.9c and 5.11c.

Table 5.3: Values of the mean heat transfer rate $\Theta'(0)$ and the mean skin friction rate $F''(0)$ for *Pr* = 0.72 and $\lambda_c = -0.13$.

ε	$\Theta'(0)$			$F''(0)$		
	$\Omega=0.2$	$\Omega=1$	$\Omega=5$	$\Omega=0.2$	$\Omega=1$	$\Omega=5$
0.000	0.7868	0.7868	0.7868	1.0792	1.0792	1.0792
0.100	0.7868	0.7868	0.7867	1.0792	1.0792	1.0793
0.200	0.7868	0.7868	0.7867	1.0792	1.0792	1.0793
0.300	0.7867	0.7868	0.7867	1.0793	1.0792	1.0793
0.400	0.7866	0.7868	0.7867	1.0793	1.0792	1.0793
0.500	0.7866	0.7868	0.7867	1.0795	1.0792	1.0793
0.600	0.7864	0.7868	0.7867	1.0796	1.0792	1.0793
0.700	0.7863	0.7868	0.7867	1.0797	1.0793	1.0793
0.800	0.7861	0.7868	0.7867	1.0799	1.0793	1.0793
0.900	0.7859	0.7868	0.7867	1.0800	1.0793	1.0793
1.000	0.7857	0.7868	0.7867	1.0802	1.0793	1.0793

Table 5.4: Values of the mean heat transfer rate $\Theta'(0)$ and the mean skin friction rate $F''(0)$ for $Pr = 6.8$ and $\lambda_c = -2.93$.

ε	$\Theta'(0)$			$F''(0)$		
	$\Omega=0.2$	$\Omega=1$	$\Omega=5$	$\Omega=0.2$	$\Omega=1$	$\Omega=5$
0.000	2.9040	2.9040	2.9040	1.6544	1.6544	1.6544
0.100	2.9039	2.9040	2.9040	1.6546	1.6544	1.6544
0.200	2.9035	2.9039	2.9040	1.6554	1.6545	1.6544
0.300	2.9028	2.9038	2.9040	1.6568	1.6548	1.6544
0.400	2.9019	2.9036	2.9040	1.6587	1.6551	1.6544
0.500	2.9006	2.9034	2.9040	1.6612	1.6555	1.6544
0.600	2.8991	2.9031	2.9040	1.6643	1.6561	1.6544
0.700	2.8972	2.9028	2.9039	1.6680	1.6567	1.6544
0.800	2.8950	2.9024	2.9039	1.6723	1.6574	1.6545
0.900	2.8924	2.9020	2.9039	1.6773	1.6582	1.6545
1.000	2.8894	2.9016	2.9039	1.6831	1.6591	1.6545

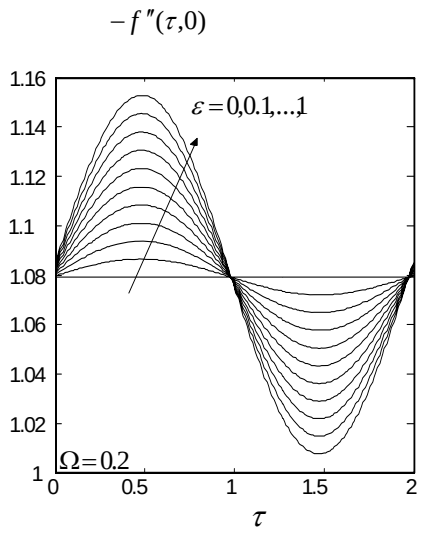

Figure 5.4a)

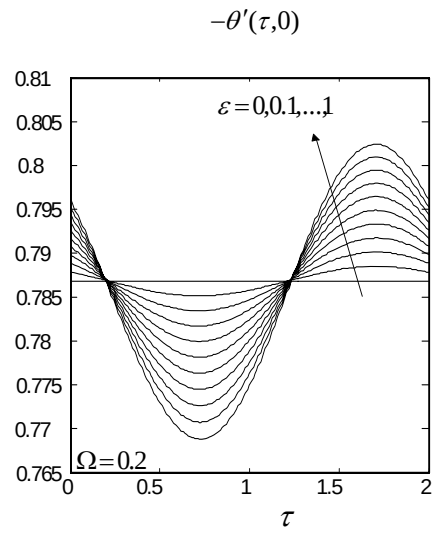

Figure 5.5a)

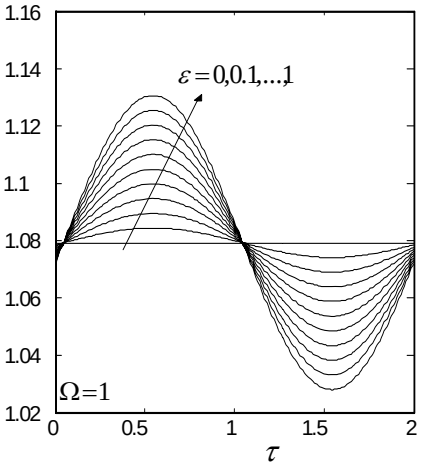

Figure 5.4b)

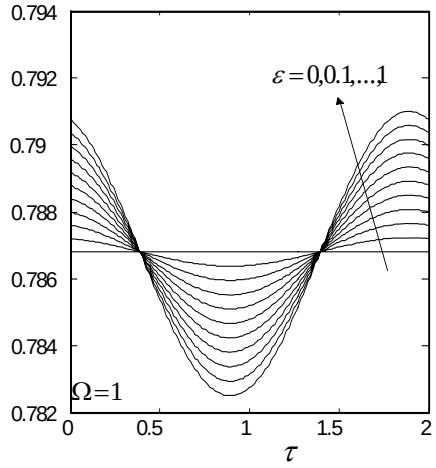

Figure 5.5b)

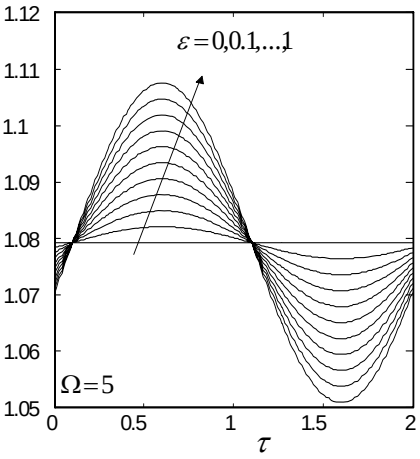

Figure 5.4c)

Figure 5.4: Variations of reduced skin friction rate for $\lambda_c = -0.13$, Pr = 0.7 and different values of ε.

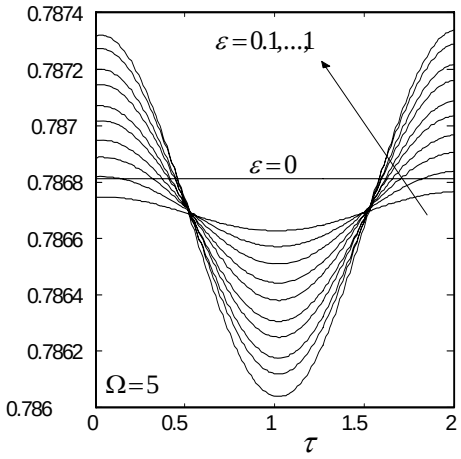

Figure 5.5c)

Figure 5.5: Variations of heat flux on the wall for $\lambda_c = -0.13$, Pr = 0.7 and different values of ε.

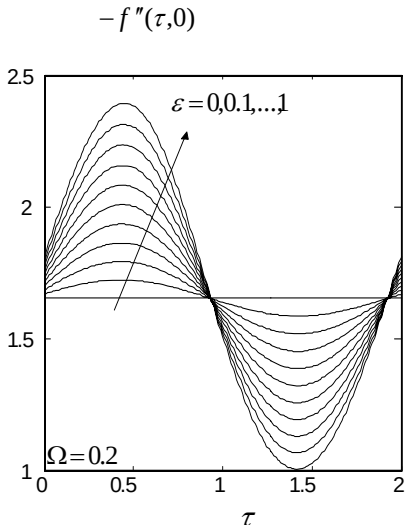

Figure 5.6a)

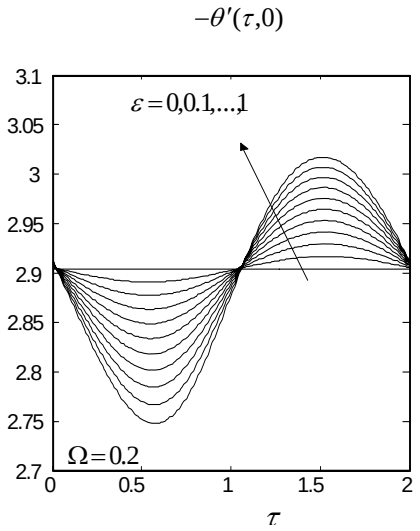

Figure 5.7a)

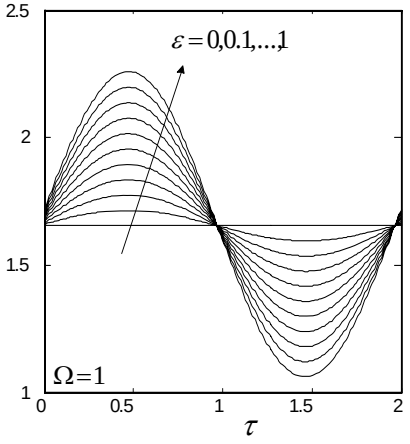

Figure 5.6b)

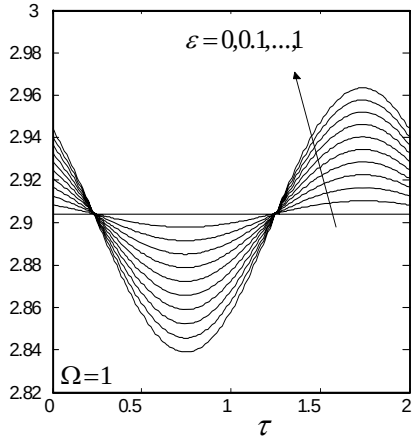

Figure 5.7b)

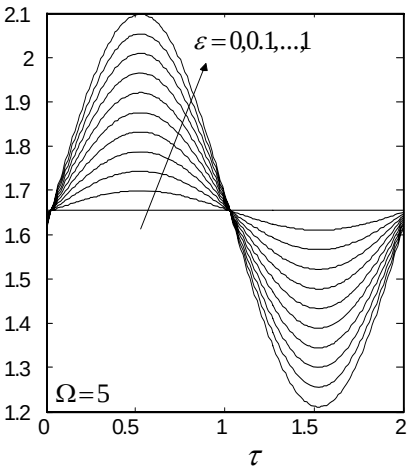

Figure 5.6c)

Figure 5.6: Variations of reduced skin friction with τ for $\lambda_c = -2.93$, Pr = 6.8 and different values of ε.

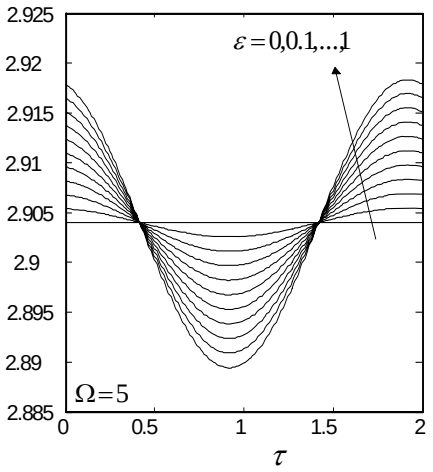

Figure 5.7c)

Figure 5.7: Variations of heat flux on the wall with τ for $\lambda_c = -2.93$, Pr = 6.8 and different values of ε.

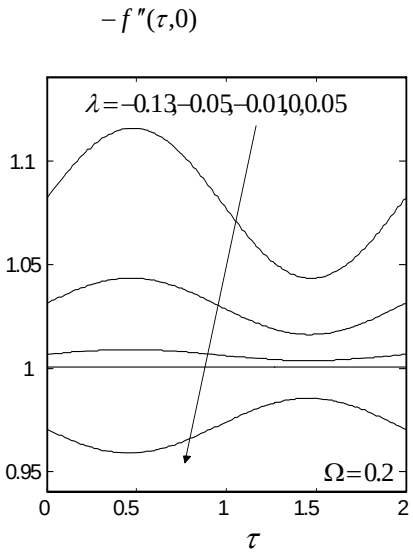

Figure 5.8a)

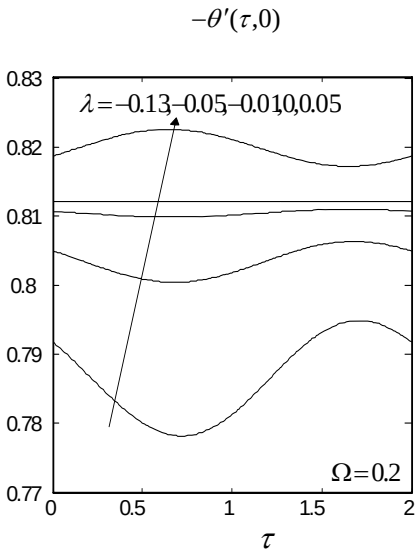

Figure 5.9a)

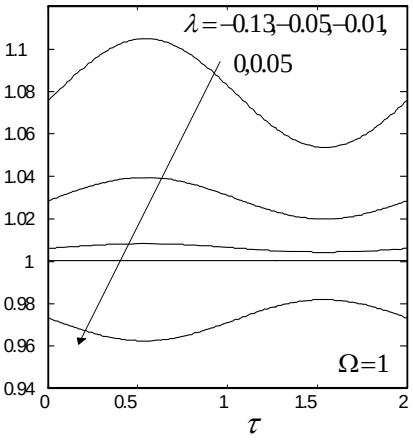

Figure 5.8b)

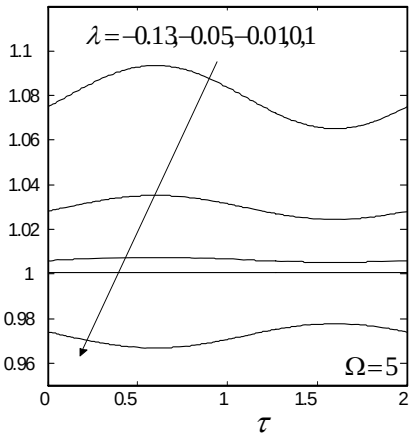

Figure 5.8c)

Figure 5.8: Variations of reduced skin friction with τ for $\varepsilon = 0.5$, Pr = 0.72 and different values of λ.

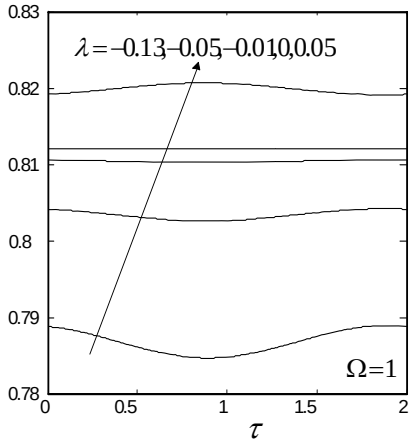

Figure 5.9b)

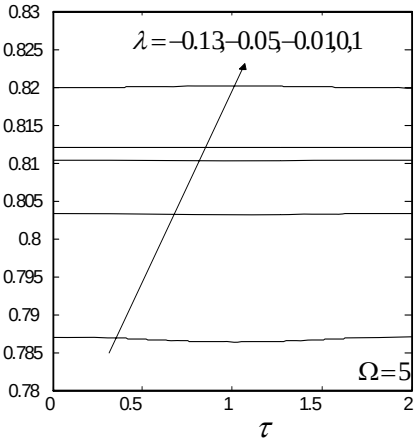

Figure 5.9c)

Figure 5.9: Variations of heat flux on the wall with τ for $\varepsilon = 0.5$, Pr = 0.72 and different values of λ.

$-f''(\tau,0)$

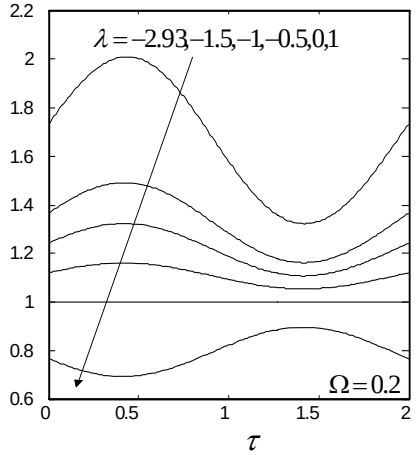

Figure 5.10a)

$-\theta'(\tau,0)$

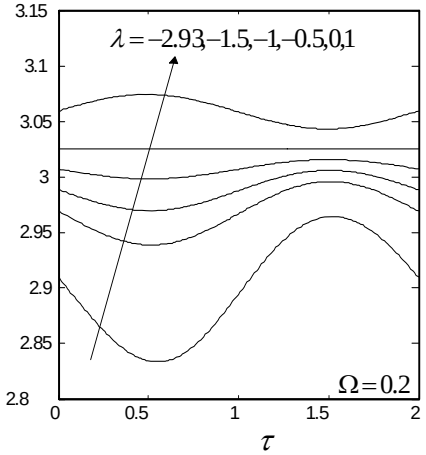

Figure 5.11a)

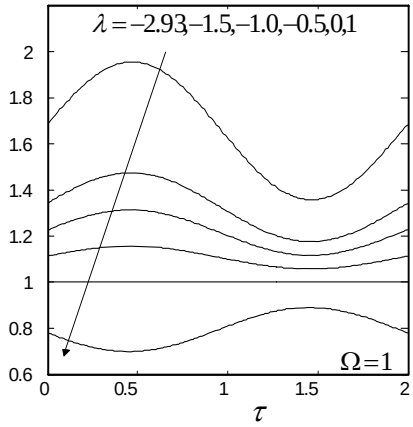

Figure 5.10b)

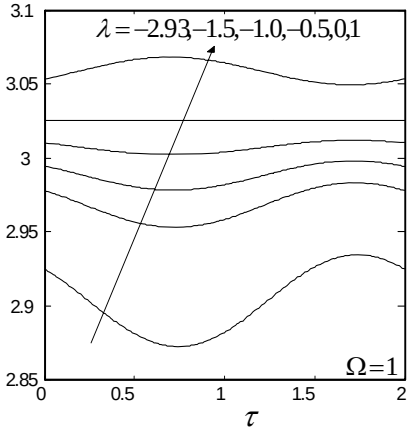

Figure 5.11b)

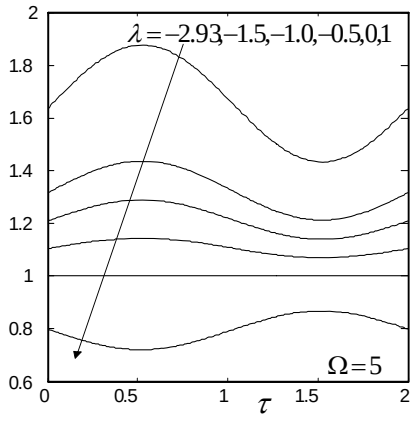

Figure 5.10c)

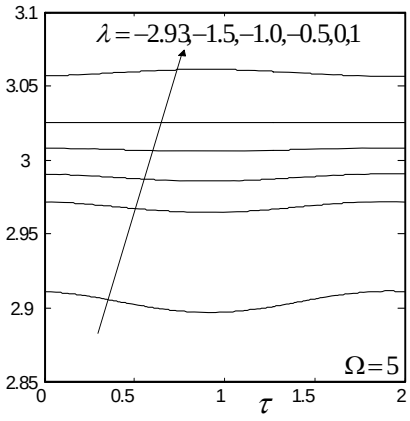

Figure 5.11c)

Figure 5.10: Variations of reduced skin friction with τ for $\varepsilon = 0.5$, Pr = 6.8 and different values of λ.

Figure 5.11: Variations of heat flux on the wall with τ for $\varepsilon = 0.5$, Pr = 6.8 and different values of λ.

CHAPTER VI

CONCLUSION

6.1 Summary of research

In this report we have considered two separate problems concerning the heat transfer coefficients of a continuous stretching surface. In the first problem, we considered the heat transfer coefficients of a continuous stretching surface subject to uniform surface temperature, variable surface temperature and uniform heat flux. The second problem considered is concerned with the effect of g-jitter induced free convection adjacent to a vertical stretching sheet. Specifically, the two dimensional, laminar and incompressible flows are considered for the first and second problems, respectively. The problems have been solved numerically using implicit finite difference method known as Keller-box method. Numerical results are presented graphically and in the forms of tables.

The first problem is discussed in Chapter IV, where we have focused on the heat transfer coefficients of a continuous stretching surface with a power law velocity and temperature distribution $-0.41 \le m \ge 3$ and for $-3 \le n \le 3$. For uniform surface temperature, $(n = 0)$ it was found that all the temperature profile, $\theta(\eta)$ exhibit asymptotic decay for all *m* (see Figures 4.1, 4.2). Furthermore, the variable surface temperature, $(n \neq 0)$ case is characterized by the variation of *n* and *m*. The magnitude of *n* affects the direction and quantity of heat flow. For example if $m = 3$ and $n = -2$ there is no heat exchange between the surface and the ambient. On the other hand, for $n > -2$ heat is transferred from continuous stretching surface to the ambient and heat is transferred to continuous stretching surface for $-3 \le n < -2$ (see

Table 4.4). Finally, for uniform heat flux, $\left(n = 0.5\left(1-m\right)\right)$, it was found that increasing *m*, increases the quantity of heat flow to the ambient. In uniform and variable surface temperature cases, the heat transfer coefficient, $Nu/\sqrt{\mathrm{Re}}$ increases with increasing *m* and Prandtl number (see Figures 4.3, 4.6, 4.7), however, heat transfer coefficient, $Nu/\sqrt{\mathrm{Re}}$ decrease with increasing *m* (see Figure 4.10). In this chapter, the plotted temperature profiles, $\theta\left(\eta\right)$ decrease with increasing Prandtl number.

In Chapter V, we have studied the problem of the effect of small but fluctuating gravitational field, characteristic of the g-jitter, on the flow and heat transfer adjacent to a vertical stretching sheet. The velocity and temperature of the sheet were assumed to vary linearly with the distance *x* along the sheet. Effects of the buoyancy parameter, amplitude of the g-jitter modulation, Prandtl number and frequency of the oscillation on the flow and heat transfer characteristics have been examined in detail. Similarity solutions have also been obtained for the case of a steady solution, case $(\varepsilon = 0)$ and it was shown that for an opposing flow these equations have solutions only for a limited range of values of the mixed convection parameter. It can be concluded that both the skin friction and the surface heat transfer increase as the mixed convection parameter increase for a given *Pr*. It is also concluded that so long as the values of *Pr* and $\lambda_c(Pr)$ are kept constant, the effect of increasing the values of ε is to give an almost proportional increase or decrease in the skin friction and surface heat transfer responses. It was also shown that for a high Prandtl number and some values of λ and Ω, the skin friction becomes more excitable than the rate of heat transfer as can be seen from Figures 5.8 to 5.11. The gravitational modulation is more effective in investigating transition from conductive to a convective temperature field at higher frequencies. It is hoped that the various induced flow behaviors predicted in this work will further serve as a well-behaved flow condition for practical microgravity processing system design and development.

6.2 Suggestions for future research

There are quite a number of interesting possibilities to continue our present research in the continuous stretching surface with power law velocity and temperature distribution. One possibility is to consider a problem in other media and effect such as micropolar fluid, effect of viscous dissipation and unsteady flow. Mohammadein and Rama (2001) considered the problem for continuous stretching surface in micropolar fluid with self similar velocity and temperature distribution using Runge Kutta method. Therefore, our research can be continuing to use the Keller box method to deal with the problem with power law velocity and temperature distribution.

On the other hand, Partha et al (2005) proposed the similarity solution for a mixed convection flow and heat transfer from an exponentially stretching surface subject to exponential velocity and temperature distribution with effect of viscous dissipation. The work of Partha et al (2005) can be extended by using the power law velocity and temperature distribution. Ishak et al (2007) studied the mixed convection on the stagnation point flow toward a vertical, continuously stretching sheet for steady flow. We can extend Ishak et al (2007) by study their problem in unsteady flow as well as the effect of g-jitter.

REFERENCES

1. Mell, W.E, Mc Grattan, K.B., Nakamura,Y., and Baum, H.R. Simulation of combustion systems with realistic g-jitter. *Sixth International Microgravity Combustion Workshop.* May 22-24, 2001. NASA Glenn Research Center, Cleveland, OH, CP-2001-210826, 2001. 333-336.

2. Yoshiaki, H., Keisuke, I., Toru, M., Satoshi, M., Shinichi, Y. and Kyoichi, K. Numerical analysis of crystal growth of an InAs-GaAs binary semiconductor under microgravity conditions. *J. Phys. D: Appl. Phys.*, 2000. 33: 2508-2518.

3. Wilcox, W.R., and Regel, L.L. Microgravity effects on material processing: A Review. *Conference Proceedings of EOROMAT 2001, Rimini, Italy*. July 10-14, 2001. Associazione Italiana di Metallurgia, 1-200121 Milano, 2001. 1-9.

4. Benjapiyaporn, C., Timchenko, V., Leornadi, E. and Davis, G.D.V.Effects of space environment on flow and concentration during directional solidification. *Int. J. Fluid Dynamics*, 2000. 4: Article 3.

5. Duval, W.M.B. and Tryggvason, B.V. Effects of G-Jitter on Interfacial Dynamics of Two Miscible Liquids: Application of MIM *37th Aerospace Sciences Meeting and Exhibit sponsored by the American Institute of Aeronautics and Astronautics, Reno Nevada*. January 11-19, 1999. Lewis Field Cleveland, Ohio: National Aeronautics and Space Administration, Glenn Research Center. 1999.

6. Boucher,R.L. Mechanically Induced g-jitter from Space Station Rotary Joints. *Spacebound Objective ESPACE 2000*. May 14-17, 2000. The Canadian Space Agency, Vancouver, British Colombia, 2000.

7. Nelson, E.S. An examination of anticipated g-jitter in Space Station and its effects on materials processes. *NASA TM 103775*, 1991.

8. Monti, R., and Sovino, R. G-sensitivity of microgravity experimentation-fundamental of disturbance response. *Microgravity and Science Technology*, 1998. 11. 2: 53-58.

9. Alexander J.I.D., Amirondine, S., Ouzzani, J., and Rosenberger, F. Analysis of the low gravity tolerance of Bridgman-Stockbarger crystal growth II: Transient and periodic acceleration: *J Cryst Growth*, 1991. 113(1-2): 21-38.

10. Kamotani,Y., Chao,L, A., Ostrach, S., and Zhang,H. Effect of g-jitter on free-surface motion in a cavity. *J Spacecraft and Rockets*, 1995. 32, n.1: 177-183.

11. Neumann, G. Three -Dimensional Numerical simulation of buoyancy-driven convection in vertical cylinders heated from below. *J Fluid Mechanics*, 1990. 214: 559-578.

12. Schneider, S.,and Straub, J. Influence of the Prandtl number on laminar natural convection in a cylinder caused by g-jitter. *Journal of Crystal Growth*, 1989. 97. n.1: 235-242.

13. Pan, Bo, Shang, D-Y., Li, B.Q. and de Groh, H.C. Magnetic field effects on g-jitter induced flow and solute transport. *Int. J. Heat Mass Transfer*, 2002. 45: 125-144.

14. Shu, Y., LI, B.Q., de Groh, H.C. Numerical study of g-jitter induced double diffusive convection in microgravity. *Numerical Heat Transfer B: Application*, 2001. 39: 245-265.

15. Ramos, J.I. Heat and mass transfer in annular jets: II. g-jitter. *Appl. Mathematics and Computation*, 2000. 110: 165-183.

16. Li,B.Q. g-Jitter induced free convection in a transverse magnetic field. *Int. of Heat and Mass Transfer*, 1996. 39: 2853-2890.

17. Li,B.Q. The effect of magnetic fields on low frequency oscillating natural convection. *Int. J. Engrg. Sci.*,1996. 34: 1369-1383.

18. Alexander, J.I.D., Garandet J.P., Favier, J.J. and Lizee, A. g-Jitter effects on segregation during directional solidification of tin-bismuth in the MEPHISTO furnace facility. *J. Crystal Growth*, 1997. 178: 657-661.

19. Jaluria, Y. *HMT The Science and Applications of Heat and Mass Transfer. Report, Review and Computer Programs*. Pergamon Press, New York. 1980.

20. Rahman M.M. and Lampinen, M.J. Numerical study of natural convection from a vertical surface due to combined buoyancies. *Numerical Heat Transfer, Part A* ,1995. 28: 409-429.

21. Rees, D.A.S. and Pop, I. g-jitter induced free convection near a stagnation point. *Heat and Mass Transfer*,2001. 37: 403-408.

22. Banks, W.H.H. Laminar free convection flow at a stagnation point of attachment on an isothermal surfaces. *Journal of Engineering Mathematics*, 1974. 8: 45-56.

23. Bhattacharyya, S. and Gupta, A.S. MHD Flow and Heat Transfer at a General Three-Dimensional Stagnation Point. *International Journal of Non-Linear Mechanics*, 1998.33: 125-134.

24. Langbein, D. Oscillatory convection in a spherical cavity due to g-jitter. *ESA Mater. Sci. under Microgravity, International Organization*, 1983: 359-363.

25. Heiss, T., Schneider, S. and Straub, J. G-jitter effects on natural convection in a cylinder: A three-dimensional numerical calculation. *ESA, Proceedings of the Sixth European Symposium on Material Sciences under Microgravity Conditions*. 1987. International Organization. 1987. 517-523.

26. Doi, T., Prakash, A., Azuma, H., Yoshihara, S. and Kawahara, H. Oscillatory convection induced by g-jitter in a horizontal liquid layer. *AIAA, Aerospace Sciences Meeting and Exhibit, 33rd.* Jan 9-12, 1995. Reno, NV, United States. 1995.

27. Okano, Y., Umemura, S. and Dost, S. G-jitter effect on the flow in a three-dimensional rectangular cavity. *Journal of Materials Processing and Manufacturing Science*. 2001. 10(1): 3-6.

28. Gresho, P.M.,and Sani, R.L. The effects of gravity modulation on the stability of a heated fluid layer. *J. Fluid Mech,*1970. 40: 783-806.

29. Biringen, S. and Peltier L.J. Computational study of 3-D Benard convection with gravitational modulation. *Phys Fluids* ,1990. A 2: 279-283.

30. Biringen, S. and Danabasoglu, G. Computation of convective flow with gravity modulation in rectangular cavities. *AIAA J. Thermophys heat transfer*, 1990. 4 :357-365.

31. Farooq, A., and Homsy, G.M. Streaming flows due to g-jitter induced natural convection. *J. Fluid Mech.*, 1994. 271 : 351-378.

32. Schlichting, H. *Boundary layer theory*. 7th. ed. McGraw-Hill: New York. 1979.

33. Lighthill, J. Acoustic streaming. *J. Sound Vib.* 1978. 61: 391-418.

34. Alexander J.I.D. Low-Gravity Experiment sensitivity to residual acceleration: A review. *Microgravity Science and Technology,* 1990. III(2): 52-68.

35. Farooq, A.,and Homsy, G.M. Linear and nonlinear dynamics of a differentially heated slot under gravity modulation. *J Fluid Mech.*, 1996. 313 : 1-38.

36. Amin, N.The effect of g-jitter on heat transfer. *Proc. R. Soc. Lond.*, 1988. A 419: 151-172.

37. Potter, J.M. and Riley, N. Free convection from a heated sphere at large Grashof number. *J. Fluid Mech.*, 1980. 100: 769-783.

38. Nazar, R., Amin, N. and Pop, I. Free convection boundary layer on an isothermal sphere in a micropolar fluid. *International Communications in Heat and Mass Transfer*, 2002. 29(3): 377 - 386.

39. Nazar, R., Amin, N. , Grosan, T. and Pop, I. Free convection boundary layer on a sphere with constant heat flux in a micropolar fluid. *International Communications in Heat and Mass Transfer*, 2002. 29(8): 1129 - 1138.

40. Beghein, C., Haghighata, F., Allard, F. Numerical study of double-diffusive natural convection in a square cavity. *International Journal of Heat and Mass Transfer*, 1992. 35: 833-846.

41. Mahajan, R.L. and Angirasa, D. Combined heat and mass transfer by natural convection with opposing buoyancies. *Transactions of ASME Journal Heat Transfer*, 1993. 115: 606-612.

42. Hussain, S., Hossain, M.A., Willson, M. Natural convection flow from a vertical permeable flat plate with variable surface temperature and species concentration. *Engineering Computations*, 2000. 17: 789-812.

43. Keller, H.B. and Cebeci,T. Accurate numerical methods in boundary-layer flows.I. Two-dimensional laminar flows.\emph{ Proc. of the second Int. Conference on Numerical Methods in Fluid Dynamics}. Springer, New York, 1971. 92-100.

44. Paterson, W.R and Hayhurst, A.N. Mass or heat transfer from a sphere to flowing fluid. *Chemical Engineering Science*, 2000. 55: 1925-1927.

45. Elperin, T. and Fominykh, A. Effect of solute concentrate level on the rate of coupled mass and heat transfer during solid sphere dissolution in a uniform fluid flow. *Chemical Engineering Science*, 2001. 56: 3065-3074.

46. Sharidan, S., Amin, N. and Pop, I. g-Jitter fully developed heat and mass transfer by mixed convection flow in a vertical channel. *International Communications in Heat and Mass Transfer*, 2005. 32: 657 - 665.

47. Jue, T.C. and Ramaswamy, B. Numerical analysis of thermosolutal flows in a cavity with gravity modulation effects. *Heat and Mass Transfer*, 2002. 38(7-8): 665-672.

48. Slouti, A., Takhar, H.S. and Nath, G. Unsteady free convection flow in the stagnation-point region of a three-dimensional body. *International Journal Heat and Mass Transfer*, 1998. 41: 3397-3408.

49. Lok, Y.Y., Amin, N. and Pop, I. Unsteady boundary layer flow of a micropolar fluid near the rear stagnation point of a plane surface. *Int. J. Thermal Sci.*, 2003. 42: 995-1001.

50. Rosenhead, D. *Laminar Boundary Layers*. Oxford University Press, London. 1962.

51. Meksyen, D. *New Methods in Laminar Boundary Layer Theory*. Pergamon, New York. 1961.

52. Wang, C.Y. Axisymmetric Stagnation Point Flow on a Cylinder. *Q. Appl. Math*, 1974.32: 207-213.

53. Sano, S and Wakitani, S. Unsteady Free Convection Near a Forward Stagnation Point at Small Prandtl Number. *Journal of the Physical Society of Japan*, 1984. 53: 1277-1283.

54. Amin N, and Riley, N. Mixed Convection at a Stagnation Point. *Quarterly Journal Mechanics and Applied Mathematics*, 1995. 48: 111-121.

55. Amin N, and Riley N. Free Convection at an Axisymmetric Stagnation Point. *Journal of Fluid Mechanics*, 1996. 314: 105-112.

56. Seshadri, R., Sreeshylan, N. and Nath, G. Unsteady Mixed Convection Flow in the Stagnation Region of a Heated Vertical Plate Due to Impulsively Motion. *International Journal of Heat and Mass Transfer*, 2002. 45: 1345-1352.

57. Nazar, R., Amin, N. and Pop, I. Unsteady Mixed Convection Near the Forward Stagnation Point of a Two-Dimensional Symmetric Body. *International Communications in Heat and Mass Transfer*, 2003. 30: 673-682.

58. Rees, D.A.S. and Pop, I. The effect of g-jitter on a free convection near a stagnation point in a porous medium. *Int. of Heat and Mass Transfer*, 2001. 44: 877-883.

59. Rees, D.A.S.and Pop, I.The effect of g-jitter on vertical free convection boundary-layer in a porous medium. *Int. comm. Heat Mass Transfer*, 2000. 27 : 415-424.

60. Rees, D.A.S. and Pop, I. The effect of large-amplitude g-jitter vertical free convection boundary layer flow in porous media. *International Journal of Heat and Mass Transfer*, 2003. 46: 1097-1102

61. Unsworth, K. and Chiam, T.C. A numerical solution of the two-dimensional boundary layer equations for micropolar fluids. *J. Appl. Math. Mech. (ZAMM)*, 1981. 61: 463-466.

62. Gorla, R.S.R., Takhar, H.S., Slaouti, A. and Pop, I. and Kumari, M. Free convection in power-law fluids near a three-dimensional stagnation point. *International Journal Heat and Fluid Flow*, 1995. 16: 62-68.

63. Peddieson, J. and McNitt, R.P. Boundary layer theory for a micropolar fluid. *Recent Adv. in Engng. Sci.*, 1970. 5: 405-476.

64. Guram, G.S. and Smith, C. Stagnation flows of micropolar fluids with strong and weak interactions. *Comp. Math.with Applics.*, 1980. 6: 213-233.

65. Lok, Y.Y., Phang, P., Amin, N. and Pop, I. Unsteady flow of a micropolar fluid near the forward and rear stagnation points. *Int. J. Engng. Sci.*, 2003. 41: 173-186.

66. Kumari, M. and Nath, G. Unsteady incompressible boundary layer flow of a micropolar fluid at a stagnation point. *Int. J. Engng. Sci.,* 1984. 22: 755-768.

67. Lok, Y.Y., Amin, N. and Pop, I. Steady two-dimensional asymmetric stagnation point flow of a micropolar fluid. *J. Appl. Math. Mech. (ZAMM),* 2003. 83: 594-602.

68. Howarth, L. The boundary layer in three-dimensional flow. Part II. The flow near a stagnation point. *Philos. Mag.*,1951. 42: 1433-1440.

69. Poots, G. Laminar free convection on the lower stagnation point on an isothermal curved surface. *International Journal of Heat and Mass Transfer,* 1964. 7: 863-873.

70. Banks, W.H.H. Three-dimensional free convection flow near a two-dimensional surface. *Journal of Engineering Mathematics,* 1972. 6: 109-115.

71. Ingham, D.B., Merkin, J.H. and Pop, I. Unsteady free convection of a stagnation point of attachment on an isothermal surface. *International Journal Mathematics and Mathematical Science*, 1984. 7: 599-614.

72. Keller, H. B. and Cebeci, T. (1972). Accurate Numerical Methods for Boundary Layer Flows, II: Two-Dimensional Turbulent Flows, *AIAA Journal*. 10: 1193-1199.

73. Cebeci, T. and Bradshaw, P. (1977). *Momentum Transfer in Boundary Layers*. Washington: Hemisphere.

74. Ali, M. E. (1994). Heat transfer characteristics of a continuous stretching surface *W¨arme Stoff¨*ubertragung. 29**:** 227–34.

75. Cebeci, T. and Bradshaw, P. (1988). *Physical and Computational Aspects of ConvectiveHeat Transfer*. New York: Springer.

76. Chen, C.H (1998). Laminar mixed convection adjacent to vertical, continuously stretching sheets. *Heat and Mass Transfer*. 33: 471–476.

77. Bejan, A. (1984). *Convection Heat Transfer*. New York: John Wiley.

78. Ghoshdastidar, P.S. (2004). Heat Transfer. Oxford University Press.

79. Ali, M E. (1995) On thermal boundary layer on a power-law stretched surface with suction or injection *Int. J. Heat Mass* Flow. 16: 280–90.

80. Crane, L.J.: Flow past a stretching plane. *J. Appl. Math. Phys. (ZAMP)*, vol. 21, p. 645 (1970).

81. Magyari, E., Keller, B.: Heat and mass transfer in the boundary layers on an exponentially stretching continuous surface. *J. Phys. D: Appl. Phys.*, vol. 32, p. 577 (1999).

82. Magyari, E., Keller, B.: Exact solutions for self-similar boundary-layer flows induced by permeable stretching surfaces. *Eur. J. Mech. B-Fluids*, vol. 19, p. 109 (2000).

83. Nazar, R., Amin, N., Pop, I.: Unsteady boundary layer flow due to a stretching surface in a rotating fluid. *Mechanics Res. Comm.*, vol. 31, p. 121 (2004).

84. Daskalakis, J.E.: Free convection effects in the boundary layer along a vertically stretching flat surface. *Canad. J. Phys.*, vol. 70, p. 1253 (1993).

85. Ali, M.E., Al-Yousef, F.: Laminar mixed convection from a continuously moving vertical surface with suction or injection. *Heat Mass Transfer*, vol. 33, p. 301(1998).

86. Chen, C.-H.: Laminar mixed convection adjacent to vertical, continuously stretching sheets. *Heat Mass Transfer*, vol. 33, p. 471 (1998).

87. Chen, C.-H.: Mixed convection cooling of heated continuously stretching surface. *Heat Mass Transfer*, vol. 36, p. 79 (2000).

88. Lin, C.-R., Chen, C.-K.: Exact solution of heat transfer from a stretching surface with

variable heat flux. *Heat Mass Transfer*, vol. 33, p. 477 (1998).

89. Chamkha, Ali J.: Hydromagnetic three-dimensional free convection on a vertical stretching surface with heat generation or absorption. *Int. J. Heat Fluid Flow*, vol. 20, p. 84 (1999).

90. Kumari, M., Slaouti, A., Takhar, H.S., Nakamura, S., Nath, G.: Unsteady free convection flow over a continuous moving vertical surface. *Acta Mechanica*, vol. 116, p. 75 (1996).

91. Antar, B.N., Nuotio-Antar, V.S.: *Fundamentals of Low Gravity Fluid Dynamics and Heat Transfer.* CRC Press, Boca Raton, FL, 1993.

92. Hirata, K., Sasaki, T., Tanigawa, H.: Vibrational effects on convection in a square cavity at zero gravity. *J. Fluid Mech.*, vol. 445, p. 327 (2001).

93. Alexander, J.I.D.: Low gravity experiments sensitivity to residual acceleration: A review. *Microgravity Sci. Techol.*, vol. III 2, p. 52(1990).

94. Nelson, E.: An examination of anticipated g-jitter on space station and its effects on material processing. *NASA Tech. Mem.*, No. 103775 (1991).

95. Amin, N.: The effect of g-jitter on heat transfer. *Proc. R. Soc. London*, vol. A 419, p. 151 (1988).

96. Farooq, A., Homsy, G.M.: Streaming flows due to g-jitter induced natural convection. *J. Fluid Mech.*, vol. 271, p. 351 (1994).

97. Li, B.Q.: **g**-Jitter induced free convection in a transverse magnetic field. *Int. J. Heat Mass Transfer*, vol. 39, p. 2853 (1996).

98. Li, B.Q.: The effect of magnetic fields on low frequency oscillating natural convection. *Int. J. Engng. Sci.*, vol. 34, p. 1369 (1996).

99. Pan, B., Li, B.Q.: Effect of magnetic fields on oscillatory mixed convection. *Int. J. Heat*

Mass Transfer, vol. 17, p. 2705 (1998).

100. Rees, D.A.S., Pop, I.: The effect of g-jitter on vertical free convection boundary layer in a porous medium. *Int. Comm. Heat Mass Transfer*, vol. 27, p. 415 (2000).

101. Rees, D.A.S., Pop, I.: The effect of g-jitter on free convection near a stagnation point in a porous medium. *Int. J. Heat Mass Transfer*, vol. 44, p. 877 (2001).

102. Rees, D.A.S., Pop, I.: g-Jitter induced free convection near a stagnation point. *Heat Mass Transfer*, vol. 37**,** p. 403 (2001).

103. Chamkha, Ali J.: Effects of heat generation on g-jitter induced natural convection flow in a channel with isothermal or isoflux walls. *Heat Mass Transfer*, vol. 39, p. 553 (2003).

104. Cebeci, T., Bradshaw, P.: *Physical and Computational Aspects of Convective Heat Transfer.* Springer, New York, 1984.

105. Grubka, L.J., Bobba, K.M.: Heat transfer characteristics of a continuous, stretching surface with variable temperature. *J. Heat Transfer*, vol. 107, p. 248 (1985).